Synthesis of Tropylium Acenes as Singlet Fission Materials for Applications in Photovoltaics

HO CHI WONG

Durham University

Department of Chemistry

Synthesis of Tropylium Acenes as Singlet Fission Materials for Applications in Photovoltaics

Ho Chi WONG

Supervisor: Dr Paul McGonigal

A project report submitted in fulfilment of the requirements for the degree of Master of Science in Chemistry by Research (2020-2022).

Abstract

Singlet fission is a process whereby one singlet excited state is converted into two triplet states, with prominent examples including acenes, namely tetracene and pentacene. These singlet fission chromophores have been widely exploited as materials for photovoltaics (PVs), as it is believed that singlet fission can help PVs overcome the Shockley−Queisser limit and increase the maximum efficiency of the devices from 33% to 45%,

This project aims to develop a synthetic route for tropylium acenes, so that they can be explored as a novel class of singlet fission chromophores with potential applications in PVs (Figure 0.1). To date, there have not been any reports which takes advantage of fused tropylium rings in functional materials. However, tropyliums possess unique characteristics which could set them apart from more common organic motifs; they exhibit remarkable stabilities relative to traditional carbocations, while their positive charges allow better charge delocalisation across the material. This fundamental area of organic materials will therefore be explored for the first time.

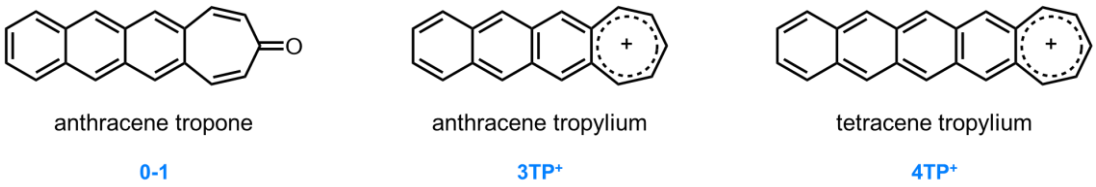

Figure 0.1. Target molecules.

Previous DFT calculations has shown that **4TP**$^+$ may have singlet and triplet energies suitable for singlet fission. Several synthetic pathways to tropylium acenes were therefore designed and tested in this work, in hopes of accessing the target molecule **4TP**$^+$. At the time of writing, however, **4TP**$^+$ has not been successfully generated.

Nevertheless, one promising pathway has provided access to anthracene tropone (**0-1**) which should be able to convert to **3TP**$^+$ via relatively common reduction and dehydration steps. This iterative pathway should allow longer tropylium acenes to be synthesised using similar methods. Once generated, the electronic and photophysical properties of these compounds, as well as their singlet and triplet energies, can be investigated spectroscopically to provide insight into these novel structures.

Acknowledgements

I would first like to express my gratitude to my project supervisor, Dr Paul McGonigal, for his invaluable support and guidance throughout this project. Even though this has been a bumpy journey which did not finish the way we had hoped, Paul's unwavering support and great patience were deeply appreciated.

I would also like to thank the rest of the McGonigal group, especially Dr Senthil Kumar for his helpful advice and ingenious suggestions, as well as Will Maturi and Promeet Saha for all the fun times in the office.

Finally, I would like to thank the ReNU CDT for funding this project.

Abbreviations

CHT	Cycloheptatriene
DFT	Density functional theory
DHA	Dihydroazuulene
FMO	Frontier molecular orbital
HOMO	Highest occupied molecular orbital
IR	Infrared
ISC	Intersystem crossing
LUMO	Lowest unoccupied molecular orbital
NBS	*N*-Bromosuccinimide
NCD	Norcaradiene
NMR	Nuclear magnetic spectroscopy
OFET	Organic field-effect transistor
OLED	Organic light-emitting diode
OPV	Organic photovoltaic
PAH	Polyaromatic hydrocarbon
PEDOT:PSS	Poly(3,4-ethylenedioxythiophene) polystyrene sulfonate
PV	Photovoltaic
SF	Singlet fission
SQ	Shockley-Queisser
TIPS	Triisopropylsilylethynyl
TP^+	Tropylium cation
$1TP^+$	Benzotropylium cation
$2TP^+$	Naphthotropylium cation
$3TP^+$	Anthracene tropylium cation
$4TP^+$	Tetracene tropylium cation
TTA	Triplet-triplet annihilation
UV-Vis	Ultraviolet-Visible
VHF	Vinylheptafulvene
VT	Variable temperature
λ_{max}	Wavelength at maximum absorption

1. Introduction

1.1 Solar Energy

Solar energy is the 'cleanest' renewable energy source available on Earth. It is an attractive option for meeting the world's energy needs, while avoiding the worst consequences of climate change induced by the combustion of fossil fuels. It is also highly abundant, as the total amount of solar energy incident on Earth is vastly in excess of the world's current and anticipated energy requirements. However, despite its great potential in satisfying all future energy needs, solar power remains a very small proportion of global electricity generation (only 3.6% as of 2022),[1] mainly because the current technologies are not capable of harnessing solar energy efficiently.

Most people are familiar with solar cells, more technically known as photovoltaics (PVs), which are electronic devices that can generate electricity directly from sunlight. The development of solar cell technology stems from the work of French engineer Edmond Becquerel in 1839,[2] who was the first to observe the photovoltaic effect during which a voltage is generated when light falls upon an electrode.[3] A few decades later, American inventor Charles Fritts created the first true solar cell by coating selenium with a thin layer of gold to capture light.[4] Although Fritts' device was too inefficient to have any practical use, his invention marked the beginning of the photovoltaic solar panel innovation. It was not until the 1950s when efficient solar energy collection by PV first appeared feasible, after researchers in Bell Laboratories developed a silicon solar cell which achieved an energy conversion efficiency of 6%.[5]

Not long after, silicon solar cells found success in space applications and became the main power source for most Earth-orbiting satellites. The first commercial solar panel power plant was built by ARCO Solar in California in 1980 after being motivated by the surge in oil prices in the 1970s.[6] Since then, researchers have continuously tried to increase the efficiencies and/or reduce the costs of solar harvesting devices, with new designs of PV using different materials such as cadmium telluride (CdTe),[7] various organic compounds, quantum dots[8] and perovskites[9] emerging throughout the years. To this day, developing cost effective solar panels remain the main goal for researchers as it is inevitable that the promise of solar power will only be fulfilled if it becomes more economically competitive.

1.1.1 Photovoltaics

A conventional solar is a bilayer device with two active materials, namely an electron donor and an electron acceptor, sandwiched between two electrodes (Figure 1.1a). The general mechanism of the energy conversion process follows four fundamental steps (Figure 1.1b).[10] The first step involves the absorption of light, when incident photons pass through the transparent front contact of the PV cell, before being absorbed by the active material. This leads to the generation of electron-hole pairs, which are also known as excitons. Once formed, the excitons diffuse to the donor-acceptor interface and dissociate into electrons (negative charge carriers) and holes (positive charge carriers). The donor-acceptor interface is also known as a p-n junction, as the "p" (positive) side contains an excess of holes, while the "n" (negative) side contains an excess of electrons. The charge carriers subsequently diffuse to the corresponding electrodes and are used to do work in an external circuit, thereby generating a current.

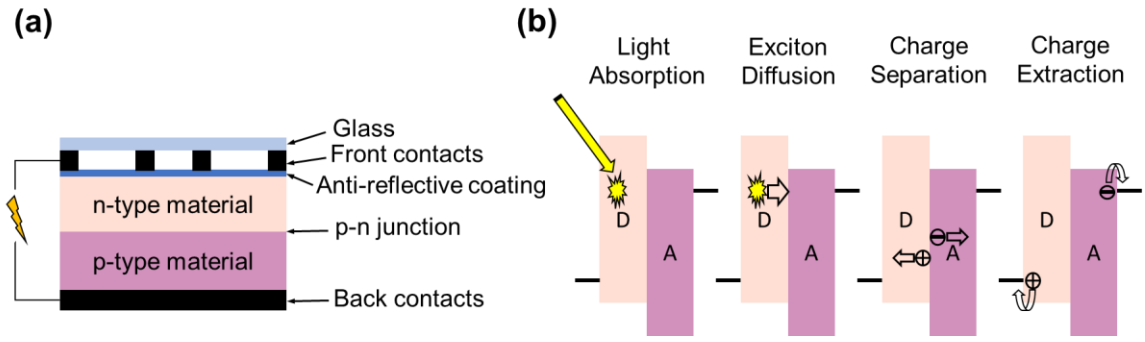

Figure 1.1. (a) Basic structure of a typical single p-n junction solar cell. (b) The general mechanism of the erny conversion process in a solar cell.

The maximum theoretical efficiency for a single p-n junction solar cell has been determined to be 33% reached at a bandgap (E_g) of 1.34 eV, a value known as the Shockley-Queisser (SQ) limit (Figure 1.2a).[11] This value was calculated by considering fundamental energy loss mechanisms in PVs. It is a valuable tool for researchers to assess PVs' energy loss channels in order to elucidate methods to improve their efficiency.[12] However, it is important to note that the SQ limit was calculated based on perfect materials containing no defects. As this assumption does not hold true in real-world conditions, the actual efficiency of PVs is often much lower than the SQ limit.

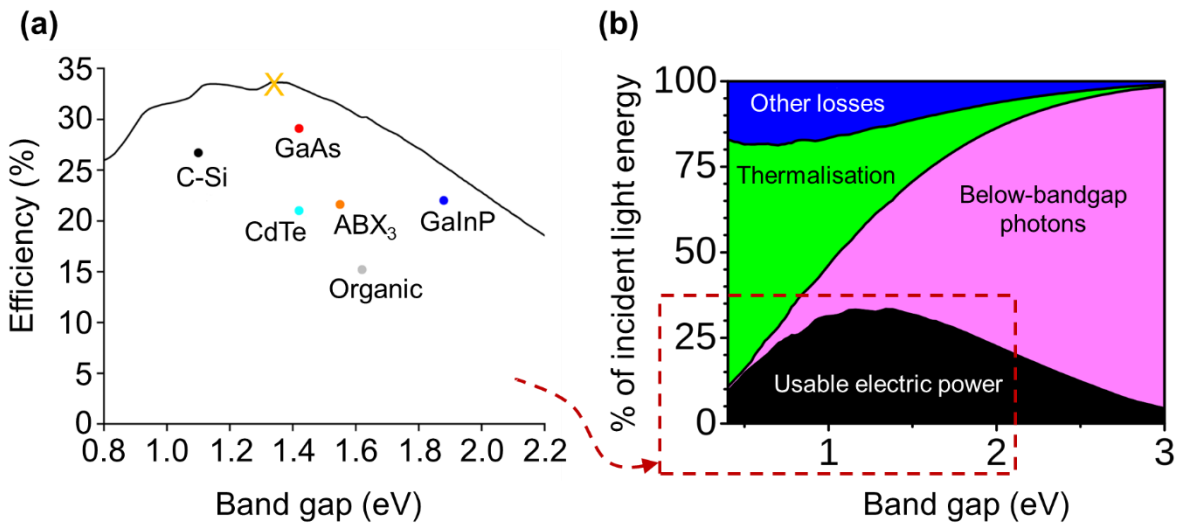

Figure 1.2. (a) Shockley-Queisser limit of efficiency (black line), with the maximum theoretical efficiency for a single p-n junction solar sell highlighted (yellow X). The highest confirmed efficiency of several major classes of solar cells are also plotted; where c-Si = crystalline silicon, GaAs = gallium arsenide, CdTe = cadmium telluride, ABX_3 = perovskite, GaInP = gallium indium phosphide.[12] (b) Proportions of energy loss mechanisms in PVs. The region highlighted (red box) corresponds to the data shown in Figure 1.2a.

The biggest energy loss in any solar cell can be attributed to the deliberate tuning of E_g, which must be large enough to generate a reasonable voltage. However, this means that photons with energy less than E_g will not be absorbed. Since a large proportion of solar radiation at ground level has energy less than the ideal PV bandgap of 1.2 – 1.4 eV, the loss of energy through the inability to absorb low energy photos is significant (Figure 1.2b).[13] The second major loss of energy is thermalisation, which is caused by the absorption of photons with energy larger than E_g. As the absorption of a single photon can only generate one electron-hole pair, when a photon with energy higher than E_g is absorbed, the excess energy is lost as heat via thermalisation.[14] Other less substantial energy loss pathways include emission losses, Carnot losses and Boltzmann losses. Emission losses are caused by the radiative recombination of electrons and holes occurring within the PV. Carnot losses occur when energy is sacrificed from converting heat energy to electrical work, which leads to a voltage drop in the device. A voltage decrease can also occur due to the Boltzmann loss, which is caused by the angular discrepancy between absorption and emission.[15]

Currently, the PV market is dominated by conventional inorganic material-based solar cells such as silicon PVs, which are relatively well-established technologies with power conversion efficiencies of approximately 25%.[16] In order to overcome the SQ limit and increase the

efficiencies of PVs, some or all of the losses described above must be eliminated. One of the more successful strategies is the use of tandem solar cells, which consist of multiple p-n junctions made of different semiconducting materials. The use of different materials allows each junction to absorb light at different wavelengths, therefore providing a broader optical window without compromising the bandgap of the material. The possible maximum theoretically efficiency for tandem solar cells is around 87% at an infinite number of junctions.[17] Experimentally, the efficiency of a six-junction system has been measured at 47%, which is one of the highest efficiencies ever achieved by a PV device.[18] However, although multi-junction solar cells have great potential in achieving high efficiencies, they are not widely used in commercial energy production due to the scarcity of raw materials required and the complex fabrication of the devices.[19]

Another possible strategy for improving PV efficiencies is to mitigate thermalisation energy losses via multiexciton generation, where two excitons are generated from one high energy photon. The most prominent example of this strategy is singlet fission (SF), a multiexciton generation process most commonly seen in organic molecules, which will be the main focus of this study.

1.1.2 Singlet fission

Over the past decades, researchers have been seeking ways to move PVs beyond their current efficiency limit and capitalise on their promised advantages. In 2006, Hanna and Nozik suggested that the implementation of multiple exciton generation, particularly singlet fission, in PVs could potentially overcome the SQ limit.[20] Singlet fission is a process in which a chromophore in an excited singlet state (S_1) shares its excitation energy with a neighbouring ground-state (S_0) chromophore and both are converted into triplet excited states ($T_1 + T_1$).[21] It is a spin-allowed process because the resulting pair of triplet states are considered to be pseudo-coupled into a singlet state (Figure 1.3).

Singlet fission was originally proposed in the 1960s to explain the time-dependent reduction of fluorescence yields observed for anthracene[22] and tetracene[23] crystals. By the mid-1970s, more sophisticated studies had been conducted on SF, as well as on the reverse phenomenon – triplet-triplet annihilation, where two triplet excitons collide and fuse into a singlet exciton.[24] Discoveries of singlet fission in new types of substrates such as carotenoids[25] and conjugated polymers[26] were subsequently made in the 1980s. However, as analytical techniques at the time

were not advanced enough to measure the quantum efficiency of SF accurately, interest in the phenomenon gradually faded and SF remained a relatively obscure topic, even within the organic photochemical community.

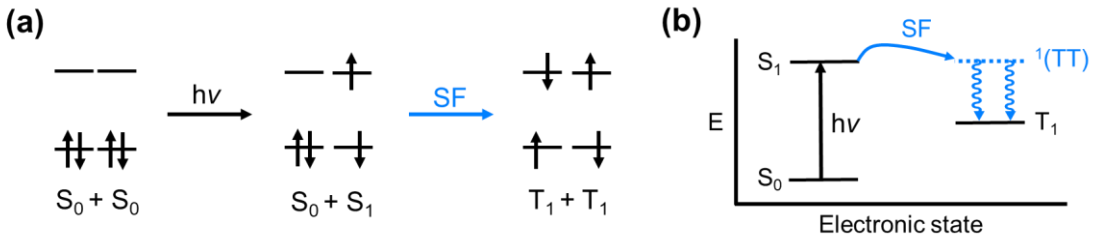

Figure 1.3. (a) A chromophore undergoes an initial excitation, then shares its energy with another ground state chromophore and creates two triplet states. (b) Simplified Jablonski diagram with the singlet fission process shown in blue.

Interest in singlet fission was relit by Hanna and Nozik when they pointed out its potential practical use in improving the efficiency of PVs. They hypothesised that if the energy of a high-energy photon can be split in two and produce two excitons that are both capable of charge separation, the excess above-bandgap energy will be better utilised and thus reducing energy loss by thermalisation. The efficiency limit of PVs can therefore potentially be increased from 33.7% to 45%.[20] Since then more studies have been devoted to investigating applications of singlet fission in PVs.

For an organic material to undergo singlet fission, it must meet all the thermodynamic requirements. In 2010, a set of fundamental guidelines for new and efficient SF materials were evaluated by Michl and co-workers.[27] First and foremost, the singlet excited state (S_1) energy of the chromophore must exceed or at least match twice the energy of the first triplet excited state (T_1):

$$E(S_1) \geq 2\,E(T_1) \qquad (1)$$

It is also important to prevent the recombination of the two triplet excited states into higher triplet excited states, which means that higher triplet excited state (T_n) energies must be higher than twice the energy of the first triplet excited state (T_1):

$$E(T_n) > 2\,E(T_1) \qquad (2)$$

Apart from these elementary requirements, other photophysical deactivation pathways must also be considered so that they do not outcompete SF. For example, SF must occur on timescales faster than its reverse reaction triplet-triplet annihilation (TTA), as well as fluorescence – the transition from the first singlet excited state (S_1) back to the ground state (S_0).[28] Materials with a rigid geometry are therefore more amenable to SF, as flexible molecules with more rotational degrees of freedom tend to relax more rapidly. On the other hand, triplet excited state population via intersystem crossing (ISC) should be supressed by using hydrocarbon materials, where ISC is negligible due to weak spin-orbit coupling.

Furthermore, when designing SF systems for PVs, additional qualities must be considered. The energy of the triplets generated by SF must match the bandgap of the device, so that they can be absorbed by the PV material.[29] The PV material must also be able to extract the triplets from the SF chromophore at the interface, as well as allowing the triplets to diffuse across the material to reach the electrodes. The orientation, crystallinity and packing of molecules all play a large role in the triplet diffusivity of PV materials.[12] More importantly, all materials used in the device must be resistant to chemical, thermal and photodegradation; they must be sufficiently stable to function over a typical PV lifespan of 25 years.[30]

The most common approach to incorporating SF materials into PVs is to use it as part of the active material of the solar cell, for example in organic photovoltaics (OPVs). OPV is a rapidly increasing bilayer solar cell technology, due to its advantages of being lightweight and relatively low material costs. However, as OPVs suffer from large device thickness due to its bilayer design, as well as being more unstable than their inorganic counterparts, the efficiencies of typical OPVs are limited to around 15%.[31] Incorporating SF materials into OPVs creates an even more difficult puzzle to solve due to the added thickness and stricter energy requirements for the device; therefore no SF-OPVs to date have outperformed optimised OPVs without SF.

The idea of an SF active material OPV means that a completely new device would have to be designed, optimised and fabricated. On the other hand, if an SF material can be added to an already optimised and efficient solar cell such as silicon PVs, efforts could be better placed elsewhere instead of re-inventing the entire device. Compounds from the acene family, namely tetracene and pentacene, have thus been widely explored as SF materials and used to augment SF-based silicon PVs, and as such this introduction will concentrate on those advances.[32,33] It should however be noted that very little work has been done on acenes longer than pentacene due to their chemical and photochemical instability, and none of it dealt with singlet fission.

1.2 Acenes

Acenes are a class of polycyclic aromatic hydrocarbons (PAHs) consisting of linearly fused benzene rings (Figure 1.4).[34,35] These compounds have long been the subject of extensive study due to their distinctive optoelectronic and semiconducting properties, which make them appealing materials for molecular electronic devices such as photovoltaics (PVs),[36] organic light-emitting diodes[37] (OLEDs) and organic field-effect transistors (OFETs).[38] They are also excellent SF chromophores as they satisfy all of the fundamental energetic requirements for SF, as described in section 1.1.2.

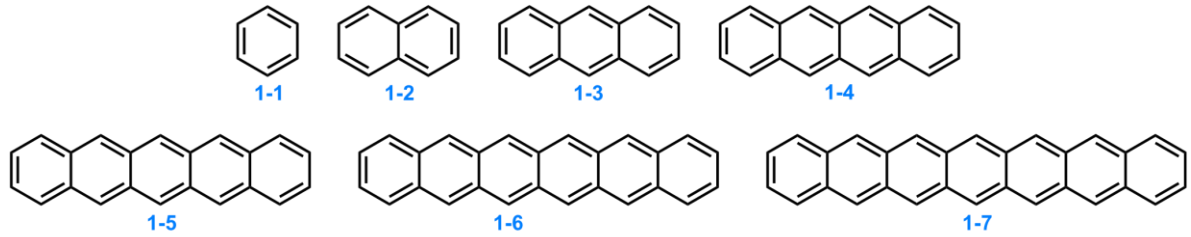

Figure 1.4. The first seven members of the acene family: benzene (**1-1**), naphthalene (**1-2**), anthracene (**1-3**), tetracene (**1-4**), pentacene (**1-5**), hexacene (**1-6**) and heptacene (**1-7**).

Benzene (**1-1**) is the smallest member of the acene family. It is famously known for possessing extra stabilising energy which arises from the delocalisation of π-electrons over multiple atoms in its planar, cyclic system, making it the epitome of the field of aromaticity. According to Hückel's seminal work in 1931,[39] the HOMOs of cyclic compounds with $4n + 2$ π-electrons (where n is an integer) have lower energies than the HOMOs of corresponding non-conjugated cyclic polyenes, and are therefore said to have aromatic character. However, while Hückel's $4n + 2$ rule successfully explained benzene's exceptional stability and accurately predicts aromaticity for monocyclic systems, its validity is limited for acenes. For example, smaller members of the acene series are stable and can be extracted from coal, while longer acenes such as pentacene (**1-5**) and hexacene (**1-6**) are not found in nature and can only be accessed by multi-step syntheses. Until very recently, higher homologues (heptacene (**1-7**) and above) have only been investigated in solid inert matrices at cryogenic temperatures.[40] A breakthrough was made in 2022 when Jančařík *et al.* reported the preparative-scale synthesis and characterisation of pure 9-ring nonacene by thermal bisdecarbonylation of precursors either in the solid-state, or in high boiling point solvents.[41] They also discovered that nonacene is surprising thermally stable up to 450 °C and does not decompose for months at room

temperature under dry argon. This success is certainly a stepping stone towards synthesising longer acenes, however, it is still yet to be proved whether this synthetic method can be applied to other homologues. To this day, the longest acene ever observed is dodecacene, a remarkable 12-ring acene generated by Moresco *et al.* on an Au(III) surface and invested using scanning tunnelling microscopy at 5 K.[42]

Instead of Hückel's $4n + 2$ rule, the unstable nature of longer acenes could be explained by a new rule proposed by Clar in 1972 as an attempt to extend Hückel's rule to PAHs, which is described in terms of aromatic sextets.[43] Aromatic π-sextets are defined as six π-electrons localised in a single benzene-like ring separated from adjacent rings by formal C−C single bonds.[44] Clar's π-sextet rule states that the resonance structure with the highest number of aromatic π-sextets is the most representative of the structure's chemical reactivity and aromaticity. However, an acene can only possess one Clar sextet regardless of the number of fused benzene rings, which spreads over the whole conjugated system (Figure 1.5). This leads to a rapid decrease in the HOMO−LUMO gap and therefore an increase in chemical reactivity with each additional fused ring.[45]

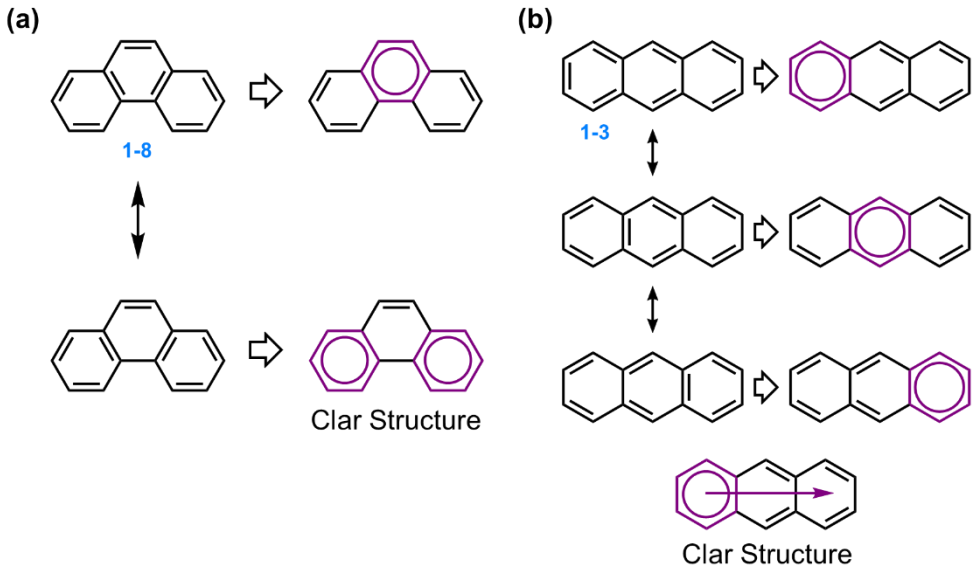

Figure 1.5. (a) Two out of five Kekulé resonance structures of phenanthrene (**1-8**) and their corresponding Clar aromatic π-sextets, indicated with a circle. The structure with the largest number of aromatic π-sextets is the so-called Clar structure. (b) Three out of the four Kekulé resonance structures of anthracene (**1-3**) and their corresponding Clar aromatic π-sextets, indicated with a circle. The Clar structure has a migrating π-sextet.

As the number of fused benzene rings increases, a reaction at the centremost ring becomes increasingly favoured as it breaks the conjugation and forms two smaller acenes of approximately the same size, each of them having its own Clar sextet (Figure 1.6).[46] Combined with their poor solubility in solvents due to their planar and rigid structure, synthesising longer acenes becomes increasingly difficult and different substituents are often required for their stabilisation.

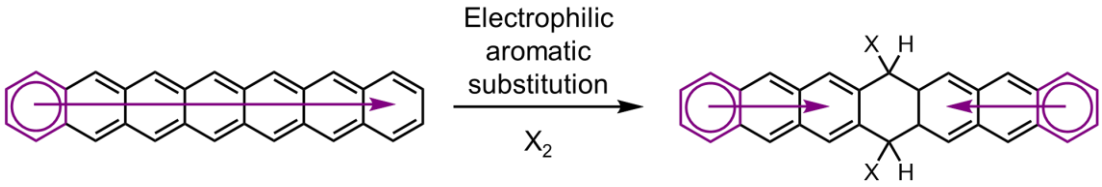

Figure 1.6. Formation of two different Clar sextets after a reaction at the centremost ring.

Acenes tend to decompose through two pathways: dimerisation or oxidation. Dimerisation occurs through a visible-light induced [4+4] cycloaddition of two acene backbones, forming a unique butterfly-shaped skeleton (Figure 1.7).[47] Such transformation for tetracene can be quickly reversed by heating, whereas the thermal reverse reaction for pentacene is much more difficult, due to the generation of a bipentacene diradical intermediate which results in larger fused-ring by-products.[48] To avoid this type of decomposition, the materials need to be isolated in an inert matrix,[49] or by forming high-quality crystals where the solid-state 'edge-to-face' arrangement sterically blocks the most reactive centremost ring, hence kinetically hindering dimerization.[46]

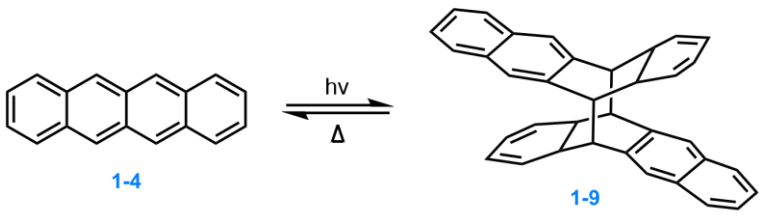

Figure 1.7. Decomposition of tetracene (**1-4**) by photodimerization.

Alternatively, acenes can react with molecular oxygen when exposed to light and air to form endoperoxides.[50] Pentacene (**1-5**) and higher acenes are particularly susceptible to photo-oxidation, but the exact mechanism is still a matter of debate. There have been reports which suggested a concerted, Diels−Alder-type process,[51] whereas a later computational mechanistic

study by Reddy *et al.* suggested that the predominant pathway involves a stepwise diradical mechanism (Figure 1.8).[52] Subsequent studies concluded that both mechanisms occur simultaneously when the acene is excited by irradiation in the laboratory, and that the rate of each reaction pathway depends heavily on the substituents on the acene backbone.[53] When the endoperoxide (**1-11**) is subjected to thermolysis or photolysis, it can either revert to the parent acene (**1-5**) via cycloreversion or transform into its corresponding quinone (**1-13**).

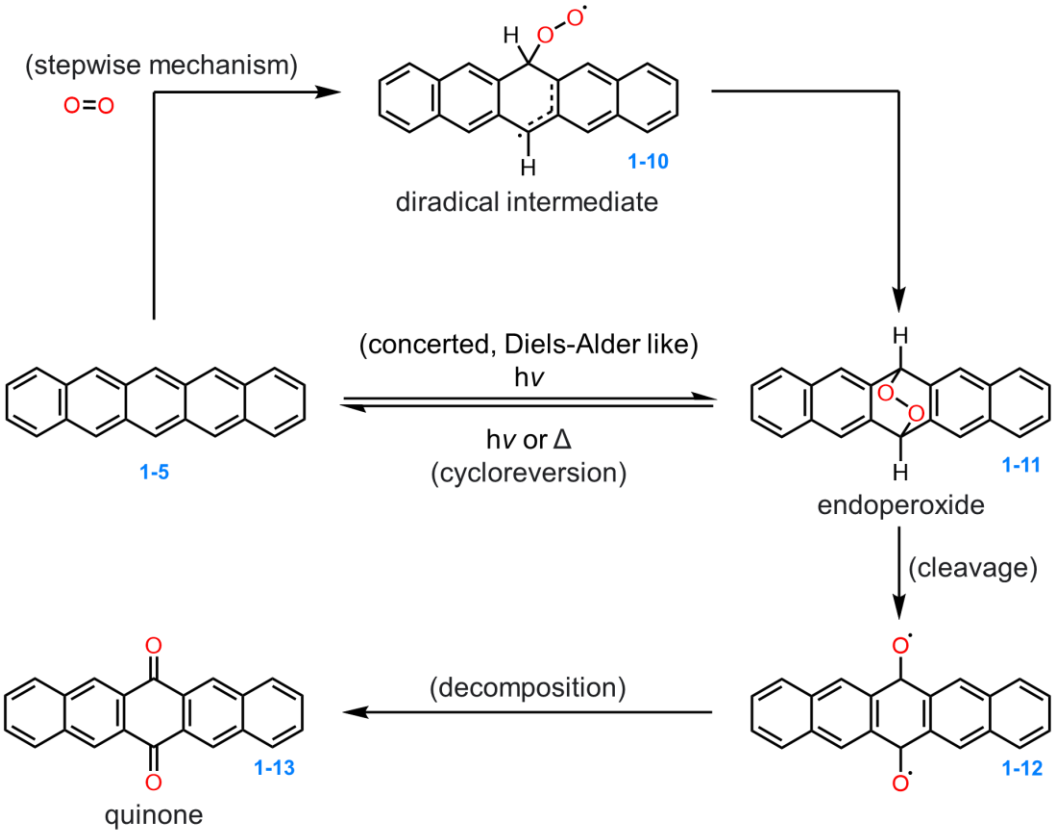

Figure 1.8. Photo-oxidation of pentacene (**1-5**) can occur via a stepwise or a concerted, Diels-Alder like mechanism to form an endoperoxide (**1-11**), which can either revert back to pentacene or transform into a quinone (**1-13**) by thermolysis or photolysis.

The instability of acenes towards both dimerisation and photooxidation can be ameliorated by attaching substituents to the conjugated core.[54] Functionalising acenes also improves their solubility and electronic properties in order to make them effective materials for molecular devices. The most common functionalisation strategies include introducing phenyl rings onto the acene core,[55] as well as the insertion of alkyne substituents with bulky trialkylsilyl moieties onto the centremost rings of acenes.[56] Crystals of 5,6,11,12-tetraphenyltetracene, also known as rubrene (**1-14**), is a notable compound used in OLEDs and OFETs, which are core elements of flexible electronic displays (Figure 1.9a).[57] The additional aryl rings in rubrene reinforce π-

stacking in the solid state, which promotes efficient charge carrier transport.[58] On the other hand, 6,13-bis(triisopropyl-silylethynyl) pentacene, more commonly known as TIPS-pentacene (**1-15**), is a well-studied pentacene analogue widely used in OFETs,[59] and have exhibited singlet fission abilities (Figure 1.9b).[60] TIPS-Pentacene is roughly 50 times more stable than the parent pentacene.[61] The bulky TIPS groups decreases the favourability of dimerisation and shields **1-15** from oxidation by blocking the centremost ring. It also possesses good electronic qualities as the favoured two-dimensional brickwork arrangement in the solid state increases the charge carrier mobilities in the material (Figure 1.9c).[62] Furthermore, the isopropyl groups on TIPS greatly increases the solubility of **1-15** in organic solvents, thus easing the synthesis of the molecule.[63] In conclusion, various functionalisation approaches can be utilised to stabilise acenes and tune their electronic properties to suit their applications in molecular devices. However, substituents must be carefully chosen to ensure the optimal packing of molecules, thus maximising their effectiveness.

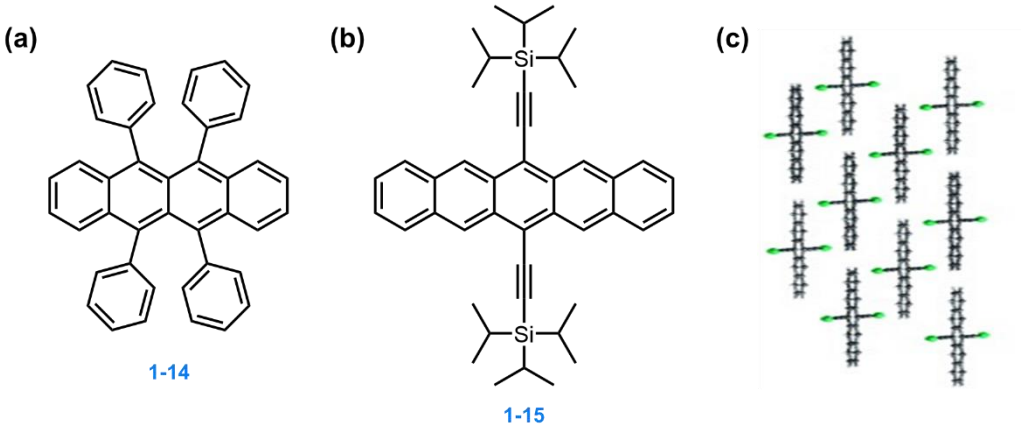

Figure 1.9. (a) 5,6,11,12-Tetraphenyltetracene, also known as rubrene (**1-14**). (b) 6,13-Bis(triisopropyl-silylethynyl) pentacene, also known as TIPS-Pentacene (**1-15**). (c) 'Brick-like' crystal packing of 1-14, shown without alkyl groups on Si for clarity.[46]

1.2.1 Acenes in photovoltaics

The desirable electronic properties of exhibited by acenes can be attributed to their arrangement in the solid state. Acenes adopt two common packing motifs – the classic 'herringbone' arrangement where the aromatic edge-to-face interaction dominates, or the coplanar arrangement in which the molecules are in a parallel-displacement π-stacking formation (Figure 1.10).[46] Both packing arrangements allow for strong intermolecular orbital overlap and hence effective electronic interactions, making them attractive materials for molecular electronic devices.

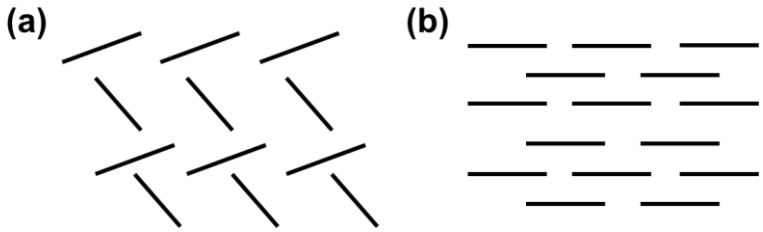

Figure 1.10. Packing motifs of acenes in the solid state: (a) herringbone or (b) coplanar.

Acenes possess a number of desirable qualities as a PV material – low molecular weight, high charge carrier mobilities, tuneable energetics, broad absorption spectra, as well as the ability to undergo singlet fission as mentioned in Section 1.1.2. For these reasons, acenes have been widely explored as SF materials and used to augment SF-based silicon PVs.

In 2018, MacQueen *et al.* evaporated 100 nm of tetracene onto an hydrogen-passivated, n-doped c-Si solar cell, before adding a polymer mixture of PEDOT:PSS[a] onto the tetracene layer as a hole transporting layer (Figure 1.11a).[32] This design was chosen to allow triplets to be harvested from tetracene at the tetracene-silicon interface, either through energy transfer or exciton dissociation. However, the triplet yield was not able to be measured directly. Simulation suggested that the tetracene layer only had an 8% exciton transfer yield, out of a possible maximum of 200%. This could be due to a potential mismatch between the silicon bandgap and tetracene triplet energy, which led to a lack of driving force for exciton dissociation in the device. It was therefore concluded at the time that the SF material did not improve the device performance.

[a] PEDOT:PSS = Poly(3,4-ethylenedioxythiophene) polystyrene sulfonate

Nevertheless, MacQueen was confident that his device is a robust platform which could potentially achieve an exciton yield of over 100%. He also suggested several pathways that can be taken to improve the solar cell design. Primarily, the triplet exciton energy of the SF layer could be tuned in order to reduce the energy mismatch between the SF layer and the silicon. On the other hand, a better interlayer could be designed to enhance exciton transfer.

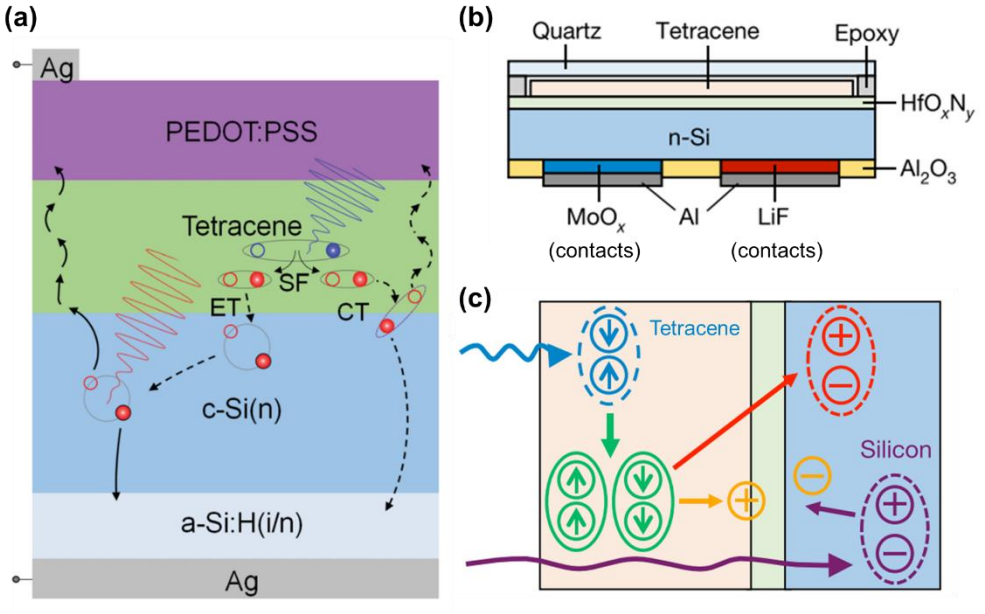

Figure 1.11. (a) Device created by MacQueen *et al.*, illustrating SF and the path of electrons (filled red circles) and holes (empty red circles). Two exciton harvesting mechanisms are depicted at the tetracene-silicon interface – energy transfer (ET) and charge transfer (CT).[32] (b) Device structure for Einzinger *et al.*'s tetracene-sensitised silicon solar cell.[33] (c) Diagram summarising the two pathways that increase silicon photoluminescence in Einzinger's device. Following the photoexcitation of tetracene (blue) or silicon (purple), exciton dissociation (orange charges) occurs at the passivating layer between the tetracene and silicon layers. Additional electron-hole pairs in silicon can also be created by singlet exciton fission in tetracene (green), followed by triplet energy transfer (red).

Currently, the thickness of interlayers poses as a practical difficulty which hinders the crucial step of transferring low-energy excitations into the solar cell. Unlike singlet excitons, triplet excitons cannot return to the ground state by fluorescence due to quantum-mechanical spin-selection rules. This restriction elongates their lifetime but at the same time prevents long-range transfer of the excitations. Singlet fission therefore cannot occur efficiently through the conventional thick passivating layer, which is added into the device to protect the solar cell from contamination and prevent rapid recombination of electrons and holes.[64] However, without this barrier, the device would suffer from power losses that overwhelm the beneficial effects of singlet fission.

More recently, Einzinger *et al.* generated an exceptionally thin passivating layer for their solar cell by growing hafnium oxynitride on top of silicon wafers using atom layer deposition.[33] This technique allowed the thickness of the layer to be controlled with high precision and the resulting layer protected the silicon surface at a thickness of only 8 Å. Apart from the remarkable passivation layer, Einzinger's SF solar cell adopted a rear-contact cell design, which was believed to be a key to high efficiency devices (Figure 1.11b). Conventional solar cells generally use opposing electrical contacts on the top and bottom of a light-absorbing semiconductor to extract electrons and holes.[64] A rear-contact (or all-back-contact) cell on the other hand is designed with both types of contact on the rear of the device, but separated. The elimination of the front surface doping allows for a wider range of texturing and light trapping schemes to be implemented on the front surface, therefore potentially increasing device efficiency.[65]

Einzinger showed that when the top tetracene layer was excited with blue or green light, triplet excitons were formed and transferred through the ultrathin hafnium oxynitride passivating layer into the silicon solar cell. Singlet excitons were also formed by the direct photoexcitation of silicon. Through photoluminescence spectroscopy, the total exciton yield was measured to be 133%, which composed of a triplet transfer yield of 76% and a singlet transfer yield of 56%. As the exciton yield, which represents the average number of excitons transferred into the solar cell photon, was greater than 1, the significant role of SF in Einzinger's device was demonstrated. However, through voltage measurements, the power conversion efficiency of their device was measured to be only 5.1%, which was significantly lower than conventional silicon PVs. At this stage, Einzinger's SF solar cell is still relatively inefficient and requires optimisation. Nevertheless, his work has certainly demonstrated the great potential in using acenes' ability to undergo SF to increase the efficiencies of silicon solar cells.

1.3 The Tropylium Cation

While the vast majority of aromatic compounds are neutral, ionic species have also shown aromatic character.[66] These lesser known analogues used to be considered of much less synthetic value as they normally possess a net charge and are likely to be less stable than benzenoid systems.[67] The beginning of the chemical history of non-benzenoid carbocyclic aromatic ions was marked in 1891 when Merling discovered the bromide salt of the cycloheptatrienyl cation, now commonly known as the tropylium cation (**TP**$^+$).[68] Other common members of the aromatic ion family include the cyclopropenium cation (**1-16**) and the cyclopentadienyl anion (**1-17**), all of which satisfy Hückel's 4n + 2 π electron rule.

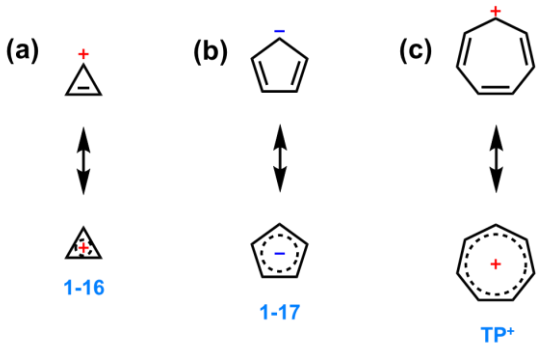

Figure 1.12. (a) Cyclopropenium cation (CH_3^+) (**1-16**) with 2 π-electrons. (b) Cyclopentadienide anion ($C_5H_5^-$) (**1-17**) with 6 π-electrons. (c) Tropylium cation ($C_7H_7^+$) (**TP**$^+$) with 6 π-electrons.

Aromatic ions can be reversibly converted into their non-aromatic neutral cyclopolyene forms by association with their counterions, and the salts formed are known to be relatively stable both in the solid state and in solution. Meanwhile, due to the reactivity of the charged systems, aromatic ions can also form covalent bonds easily with other substrates to afford reactive intermediates, which have the tendency to rearomatize and thus provide the driving force for chemical reactions.[69] This unique combination of stability (as a result of aromaticity), and reactivity (which arises from the associated net charge) allows aromatic ions to be used in a wide range of reactions. One of the most notable examples, **1-17**, which is formed by deprotonation of cyclopentadiene, has been widely exploited as an η^5-ligand in organometallic complexes with versatile catalytic properties.[70]

The tropylium cation (**TP**$^+$) is a seven-membered cyclic ion with six π-electrons delocalised via an empty p_z orbital, leading an overall charge of 1+. Its salts were first obtained by Merlin in 1891 from the reaction of cycloheptatriene (C_7H_8) (**CHT**) and bromine.[68] Unlike most

hydrocarbyl bromides, the compound formed was water-soluble but insoluble in many organic solvents. It also reacted with aqueous silver nitrate immediately to form silver bromide, indicating the bromide was labile. However, Merlin did not know the structure of the compound at the time, nor did he know the compound was a salt. It was not until 1954 when Doering and Knox deduced tropylium bromide (**1-18**) to be a salt, $C_7H_7^+Br^-$, and characterised it by IR and UV-vis spectroscopy.[71] Subsequent X-ray crystallography studies by Hoffmann *et al.* revealed a planar structure with seven equivalent C−C bonds of bond length 1.39 Å, thereby confirming the aromaticity of **TP**$^+$.[72] The high symmetry of **TP**$^+$ (point group D_{7h}) was also reflected by its small number of IR and Raman absorption bands.[73]

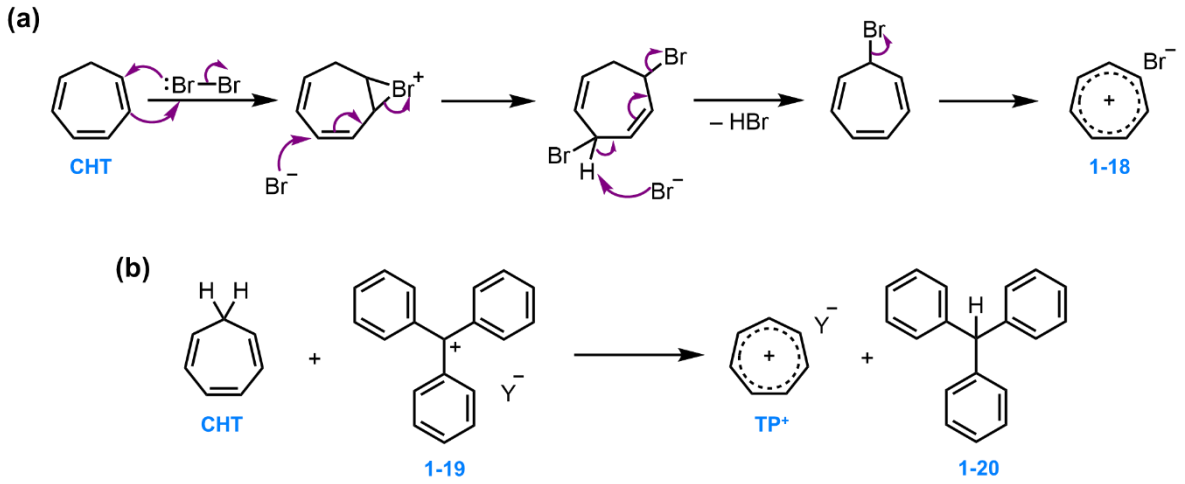

Figure 1.13. (a) Doering's method of reacting **CHT** with bromine to generate tropylium bromide (**1-18**). (b) Dauben's method of reacting **CHT** with tritylium salts (**1-19**) to generate a series of **TP**$^+$ salts.

Over the years, different methods and conditions have been developed for the synthesis of **TP**$^+$, with varying degrees of success. The aforementioned method developed by Doering involved direct oxidation of unsubstituted **CHT** by employing bromine as an oxidant (Figure 1.13a).[71] Subsequently, Dauben *et al.* reported a novel method of generating a series of **TP**$^+$ salts by hydride exchange reactions using trityl (triphenylcarbenium) salts (**1-19**) in 1957 (Figure 1.13b).[74] By reacting **CHT** and trityl salts with different counterions in acetonitrile at room temperature for only several minutes, pure **TP**$^+$ perchlorate, tetrafluoroborate and halide salts were obtained in good yields of 60−90%. Apart from direct oxidation from **CHT**, substituted **CHTs** can also be used as precursors for **TP**$^+$ salts. For example, an approach involving the treatment of cycloheptatrienol[75] or 7-methoxy **CHT**[76] with tetrafluoroboric acid to afford the tetrafluoroborate salts was developed in later years. On the other hand, an alternative electrochemical oxidation was demonstrated by Geske in 1959, who achieved oxidation by

applying a voltage of +1.13 V to a solution of **CHT** in acetonitrile (vs. Ag / $AgNO_3$) using a platinum electrode.[77] The formation of $\mathbf{TP^+}$ was confirmed as the absorption spectrum of the electrolysed solution was identical to the spectrum of tropylium perchlorate. Nevertheless, the most common synthetic strategy to access $\mathbf{TP^+}$ revolves around the oxidation of **CHT** derivatives.

1.3.1 Cycloheptatriene

Cycloheptatriene (previously known as tropylidene) is a non-planar, non-aromatic, seven-membered carbocycle consisting of a conjugated triene and an sp^3-hybridised methylene bridge. In its ground state, the methylene group sits above the plane of the triene, resulting in a boat conformation (**1-21**) which can interconvert through a planar transition state (**1-22**) to an inverted boat structure (**1-23**), with an energy barrier of ~24 kJ mol^{-1} (Figure 1.14a).[78] Through calculations from the microwave spectrum of **CHT**, the out-of-plane angles at the bow and the stern of the boat were reported to be $\theta = 50°$ and $\varphi = 30°$ respectively by Butcher *et al.* (Figure 1.14b),[79] which were supported by subsequent *ab initio* DFT calculations performed by Donovan and White.[80]

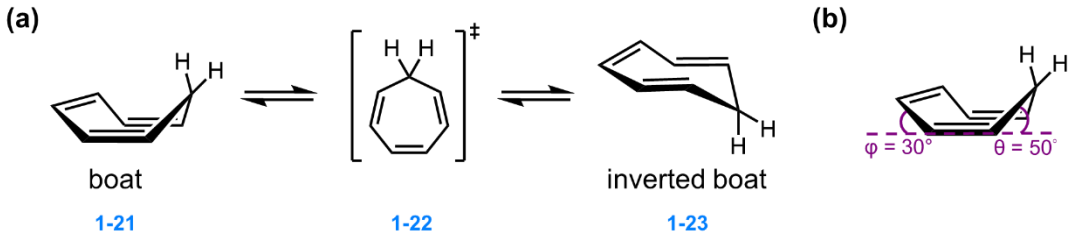

Figure 1.14. (a) Conformational interconversion of **CHT**. (b) Ground-state geometry of **CHT** with out-of-plane angles of 30° and 50°.

CHT was first generated by Ladenburg in 1881 via the decomposition of tropine.[81] However, its structure remained unknown until two decades later, when Willstätter reported its characterisation and synthesis from cycloheptanone.[82] Over the following century, **CHT** played an integral part in organometallic chemistry as an η^6 ligand (**1-24**),[83] and also in rotaxane chemistry as a donor station (**1-27**).[84] Although less common than its aromatic homologue benzene, **CHT** is found in the carbon framework of a diverse range of natural products, such as colchicine (**1-25**), a treatment for gout and Bechet's disease, as well as thujaplicins (**1-26**), which are known for their antibacterial properties.[85]

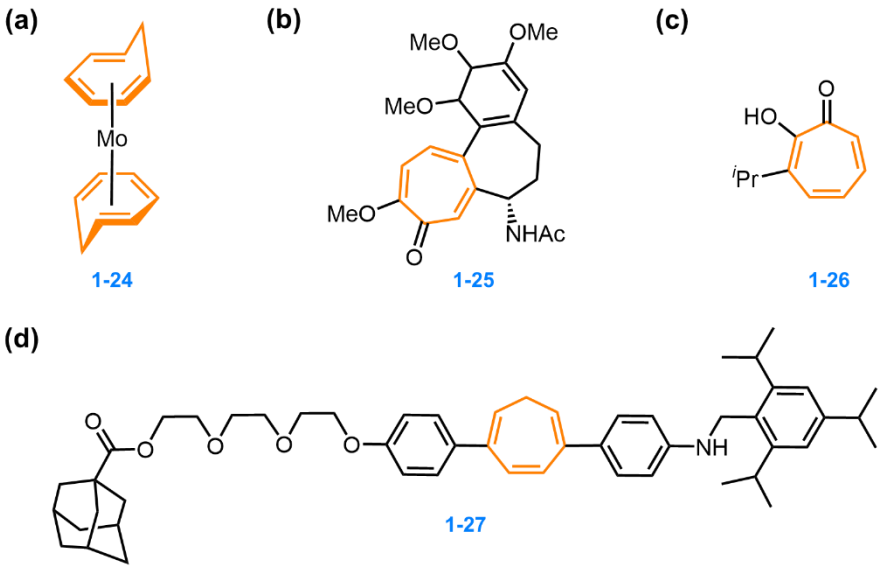

Figure 1.15. Examples of structures containing **CHT**s (highlighted in orange). (a) Mo(η^6-C_7H_8)$_2$ complex. (b) Colchicine. (c) α-Thujaplicin. (d) Molecular thread containing a diaryl-**CHT** station, which is used to make rotaxanes.

1.3.1.1 Buchner ring expansion

Buchner and Curtius began investigating the addition of carbenes to benzene in 1885, in hopes of accessing novel **CHT**s.[86] The carbenes they used were generated from the *in situ* thermal decomposition of α-diazocarbonyl compounds, a method which was reported by Curtius himself two years earlier (Figure 1.16).[87] During their study, the products from the reaction of ethyl diazoacetate (**1-28**) in benzene were discovered to be ethyl-7-norcaradienecarboxylate (**1-29**), as well as three isomeric **CHT** ethyl esters (**1-30b–d**). This synthetic route, now famously known as the Buchner ring expansion, is still regarded as one of the most powerful means of preparing **CHT**s from functionalised aromatics to this day.

The Buchner ring expansion proceeds via a [2+1] cycloaddtion between the carbene intermediate and a double bond in benzene to form a norcaradiene (**NCD**) intermediate, which undergoes a thermally allowed disrotatory electrocyclic ring opening to form the more stable **CHT** tautomer[b].[88] The three isomers of **1-30a** were formed by subsequence isomerisation through [1,3] sigmatropic shifts. Since the reaction's first discovery, transition metal catalysts,

[b] While norcaradiene (**NCD**) and cycloheptatriene (**CHT**) are valence isomers, the interconversion is commonly described as **NCD–CHT** tautomerisation,[138] and accordingly, this terminology is used throughout this report.

most notably rhodium(II) catalysts, have been used to optimise the Buchner reaction by stabilising the carbene intermediate.

The use of dimeric rhodium(II) carboxylates as catalysts for the Buchner ring expansion was first discovered by Anciaux *et al.* in 1981.[89] They discovered that the presence of strongly electron-withdrawing ligands on the rhodium ion promoted the formation of highly electrophilic carbenes, which showed a large selectivity for the addition to benzene than to its non-aromatic counterpart, cyclohexene. Further screening studies have since been carried out, resulting in the rhodium(II) trifluoroacetate dimer, $[Rh_2(CF_3COO)_4]$, becoming the most widely employed catalyst as it has been shown to increase reaction yields up to more than 90%.[90]

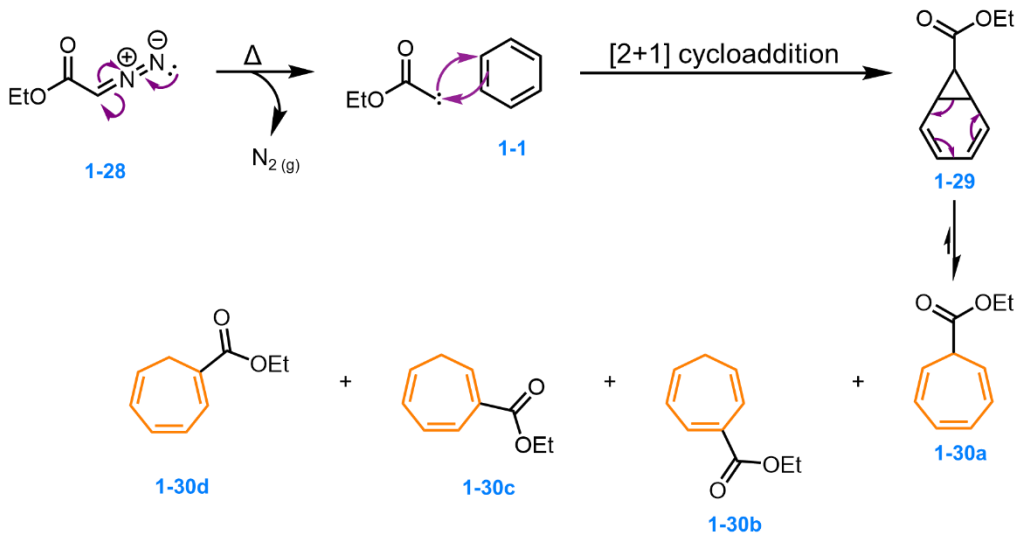

Figure 1.16. Mechanism for the Buchner ring expansion of benzene by reaction with ethyl diazoacetate (**1-28**). The three isomeric isomers (**1-30b–d**) are formed by [1,3]-sigmatropic shifts of **1-30a**.

Although Buchner claimed that the **CHT** isomers were formed via the **NCD** tautomer, **NCD**'s existence was much disputed as he was not able to isolate it. Since then various groups have studied the **NCD-CHT** equilibrium in depth, but in the following decades stable **NCD**s were only obtained either by incorporating one or both of its double bonds into an aromatic system (**1-31** and **1-32**),[91] or by adding an additional 3-atom bridge between C_1 and C_6 (**1-33**).[92] Initial variable temperature (VT) ^{1}H NMR studies on **CHT** also failed to provide proof of **NCD**'s existence at temperatures as low as −150 °C, but they did give more detailed insight into the non-planar geometry of **CHT** and its interconversion between the two boat conformations.[93] It was not until the mid-1960s that Assour and Harrison reported the formation of 7,7-

dicyanonorcaradiene (**1-34**),[94] exclusively in the **NCD** form, from the thermolysis or photolysis of dicyanodiazomethane in benzene with a yield of 80%, and confirmed its structure by ^{1}H NMR spectroscopy. Subsequently, Wehner and Guenther successfully observed a 97:3 mixture of **CHT:NCD** in dynamic equilibrium at −151 °C by ^{13}C NMR in 1975.[95]

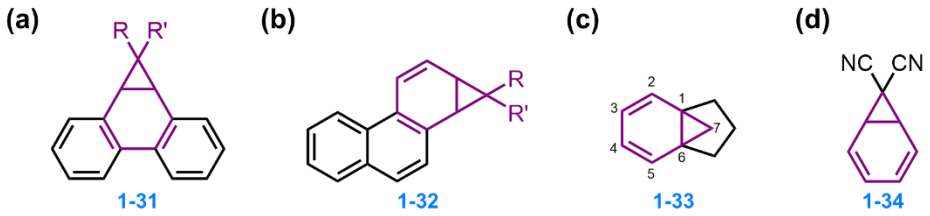

Figure 1.17. Closest attempts of a stable **NCD** synthesised during the first half of the 20th century.

Once the **CHT-NDC** equilibrium had been established and confirmed, research on **CHT**s started shifting towards investigating substituent effects on the equilibrium position (Table 1.1). Generally, the **CHT** tautomer is favoured over **NCD** in simple systems due to the strained cyclopropane ring. However, the dicyano compound (**1-34**) reported by Assour and Harrison was a stable **NCD**.[94] This observation was justified by Hoffmann's postulate that π-acceptors can interact with the HOMO of the cyclopropane ring, thus stabilising the ring by delocalising electrons over the π-system.[96] Conversely, π-donors donate electrons into the cyclopropane ring's LUMO, increase the anti-bonding character of the ring and therefore destabilise it. A few years later, computational study published by Clark *et al.* augmented Hoffmann's theory by addressing substituents with σ-character.[97] It was claimed that σ-donation into the σ-antibonding molecular orbital of the cyclopropane ring shortens the C_1−C_6 bond and elongates the C_1−C_7 bond, therefore stabilising the ring and favouring the **NCD** tautomer, while σ-acceptors have the opposite effect. Fluorine substituents such as CF_3 were believed to act predominantly as σ-acceptors not as π-donors.

Table 1.1. Effects of substitution in the C_7 position on the **NCD**−**CHT** tautomeric equilibrium.

R	Type	Major Tautomer
H	–	CHT
CN	π-acceptor	NCD
OMe	π-donor	CHT
CF_3	σ-acceptor	NCD
*i*Pr	σ-donor	CHT

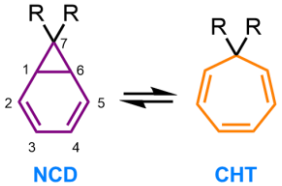

While the Buchner ring expansion provides a convenient synthetic route towards **CHT**s, its scalability is limited due to the need for expensive and non-reusable rhodium catalysts. Moreover, the harsh conditions required to facilitate carbene formation, coupled with the high reactivity of carbenes, often lead to poor chemoselectivity or unwanted side reactions, especially in more complex structures.[98] As a result, alternative routes have been explored to optimise the synthesis of **CHT**s.

1.3.1.2 Cycloadditions

A cycloaddition reaction is a concerted, pericyclic reaction which forms a cyclic adduct between two or more π-reactants, through the formation of two new σ-bonds and two fewer π-bonds.[99] Owing to its ability to form multiple bonds in a single reaction, cycloadditions have been a popular synthetic route for complex cyclic molecules. Depending on the symmetry of overlapping π-orbitals of the reactants, the reaction proceeds either via a thermal or photochemical route. In the mid-1960s, a set of generalised rules applicable to all pericyclic reactions were put forward by Woodward and Hoffmann to predict easily whether a reaction is symmetry-allowed or symmetry-forbidden, and hence whether it is thermally or photochemically allowed.[100] These rules allow the reaction mechanism to be understood in terms of the frontier molecular orbital (FMO) theory, which only takes into account the HOMO−LUMO interactions between reacting molecules (Table 1.2). The interactions or orbitals are described as either suprafacial, where the interaction occurs on the same face, or antarafacial, where opposite faces interact.

Table 1.2. Summary of the Woodward-Hoffmann rules for cycloadditions.

Number of π-electron pairs	Thermally allowed overlap	Photochemically allowed overlap
Odd (4n + 2)	suprafacial – suprafacial	suprafacial – antarafacial
Even (4n)	suprafacial − antarafacial	suprafacial − suprafacial

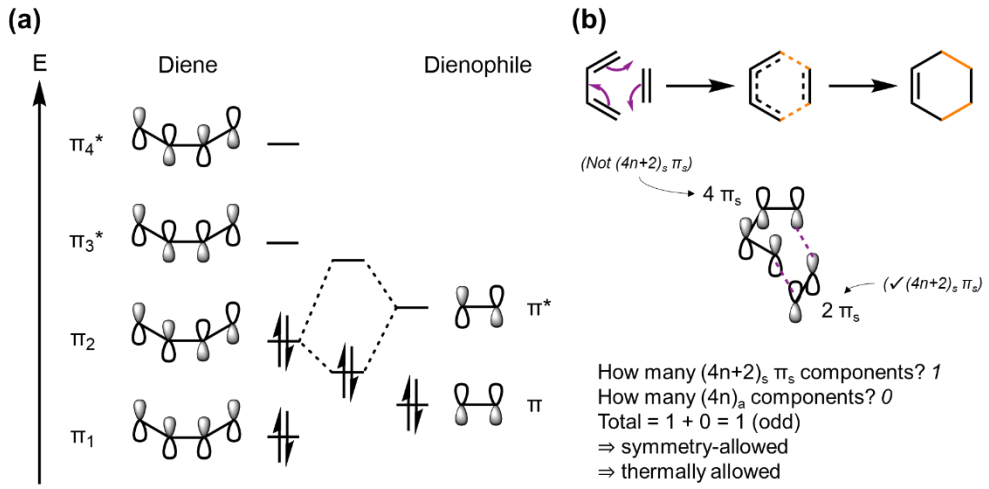

Figure 1.18. (a) Interactions between FMOs in a thermally allowed [4+2] cycloaddition. (b) Mechanism of the Diels-Alder cycloaddition showing suprafacial orbital overlap.

One of the most explored pericyclic reactions for the synthesis of **CHT**s is A Diels-Alder reaction – a thermally allowed, concerted [4+2] cycloaddition of a conjugated diene (4 π-electrons) and a dienophile (2 π-electrons). In this reaction, the diene's HOMO interacts with the dienophile's LUMO suprafacially, forming two C−C σ-bonds simultaneously. **CHT**s can be generated by using cyclopentadienone derivatives (**1-35**) as dienes and cyclopropenes (**1-36**) as dienophiles (Figure 1.19). The reaction proceeds via tricyclic intermediate (**1-37**), and is entropically driven by the subsequence loss of CO gas through a chelotropic cycloreversion to form the **NCD** (**1-38**), which eventually rearranges into a **CHT**.

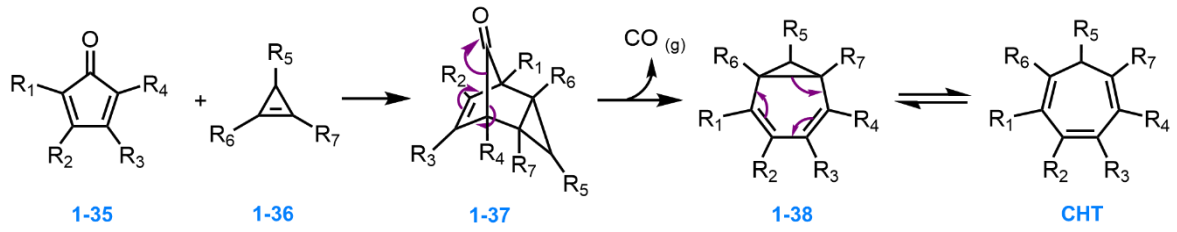

Figure 1.19. Mechanism of a general Diels-Alder reaction to form functionalised **CHT**.

A notable study by Reinhoudt *et al.* in 1973 provided an alternative strategy to access **CHT**s by using modified thiophene dioxide substrates (**1-39**), via an inverse electron demand Diels-Alder reaction (Figure 1.20).[101] In this reaction, the electron-deficient diene's LUMO overlaps with the dienophiles's HOMO to form a tricyclic adduct (**1-41**), which loses SO_2 gas rapidly to afford the desired **CHT** with a high yield of over 95%.

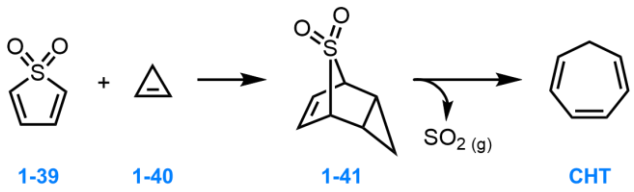

Figure 1.20. Reinhoudt's synthesis of CHT's.

Functionalised **CHT** can also be synthesised by less common cycloadditions using transition metal catalysis. Examples of [3+2+2] cycloadditions between alkynes and allylic alcohols using π-allyl nickel,[102] palladium[103] and ruthenium[104] complexes have all been reported. On the other hand, a [2+2+2+1] cycloaddition between naphthoquinones (**1-42**) and *N*-(acylmethyl) pyridinium iodide (**1-43**), mediated by Mn(II) under mild conditions has also been reported as a method to prepare more complex structures with a **CHT** core (**1-44**) (Figure 1.21).[105]

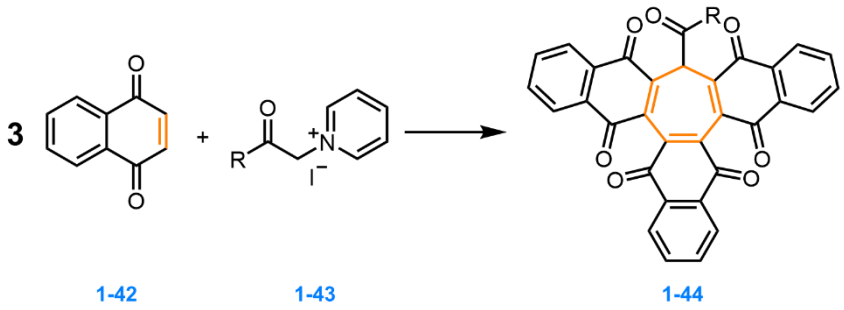

Figure 1.21. A [2+2+2+1] cycloaddition between naphthoquinones (**1-42**) and *N*-(acylmethyl) pyridinium iodide (**1-43**) to form a complex structure **1-44** with a **CHT** core.

1.3.2 Tropylium acenes

The first tropylium acene was reported by Heilbronner *et al.* in the 1950s.[106] Throughout that decade his research group carried out intensive studies on a large series of benzologue tropones and tropylium cations (Figure 1.22). They reported the syntheses of benzo-, dibenzo-, naphtho-tropones and tropylium cations, as well as their physical-chemical properties such as electronic spectra, heats of formation, dipole moments and relative acidities.[107] Nevertheless, even though these compounds have been studied extensively by Heibronner, there has not been much interest on these structures since they were first discovered.

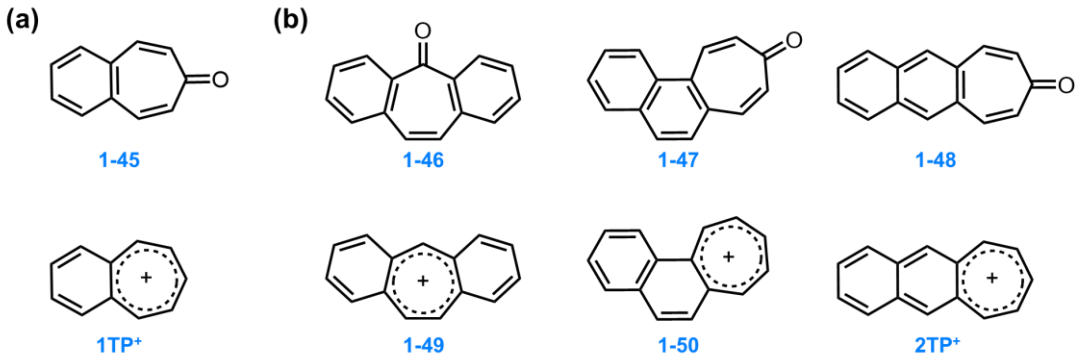

Figure 1.22. (a) Benzotropone (**1-45**) and its corresponding benzotropylium cation (**TP**$^+$). (b) Benzologues of tropone (**1-46 – 1-48**) and tropylium cations (**1-49 – 1-50** and **2TP**$^+$), synthesised by Heibronner *et al.*.

Heilbronner's synthetic route towards the napthotropylium cation (**2TP**$^+$) involved a Knoevanagel condensation between 2,3-naphthalenedicarboxaldehyde (**1-51**) with diethyl-1,3-dicarboxlate (**1-52**), followed by decarboxylative hydrolysis to remove the two ester groups (Figure 1.23). The naphthotropone (**1-48**) obtained was reduced to the corresponding alcohol (**1-54**) with lithium aluminium hydride, which was treated with a Brønsted acids such as perchloric acid or sulfuric acid to generate **2TP**$^+$.[108]

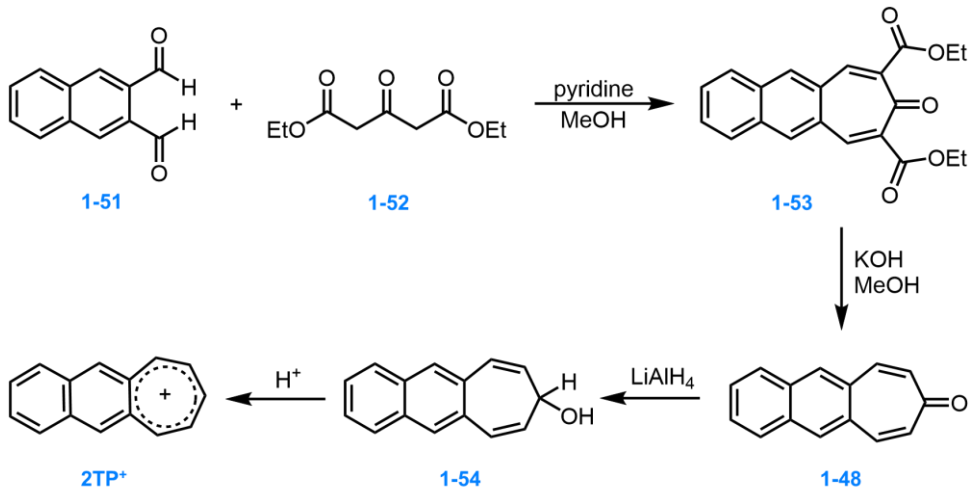

Figure 1.23. Heilbronner's synthesis of 2TP$^+$ via Knoevenagel condensation.

A decade later, Srivastava reported a slightly different synthetic route for **1TP**$^+$, which he came across serendipitously during his attempt to synthesise and study the equilibrium system shown in Figure 1.24:[109]

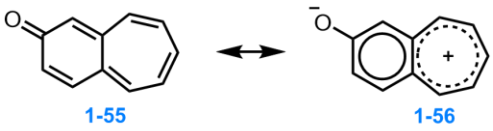

Figure 1.24. The equilibrium system Srivastava was trying to synthesise before he serendipitously synthesised **1TP**$^+$.

Srivastava's method involved reacting benzosuberene (**1-57**) with one equivalent of *N*-bromosuccinimide (NBS) in refluxing CCl_4, which generated an unstable bromo derivative (**1-58**) by allylic bromination (Figure 1.25). Upon working-up, **1-58** was discovered to have eliminated HBr and formed 1,2-benzocycloheptatriene (**1-59**). **1-59** was then reacted with NBS in refluxing CCl_4 again in hopes of generating a second bromo-derivative (**1-61**), which was expected to give the corresponding benzotropylium salt when treated with $AgClO_4$ in nitromethane, based on an earlier report by Berti.[110] However, it was discovered that the second allylic bromination with **1-59** did not generate the desired **1-61**, but instead a succinimide adduct (**1-60**). Fortunately, **1-60** turned out to be an excellent, stable precursor for **1TP**$^+$, generating benzotropylium perchlorate with a 60% yield readily when treated with perchloric acid in acetic anhydride.

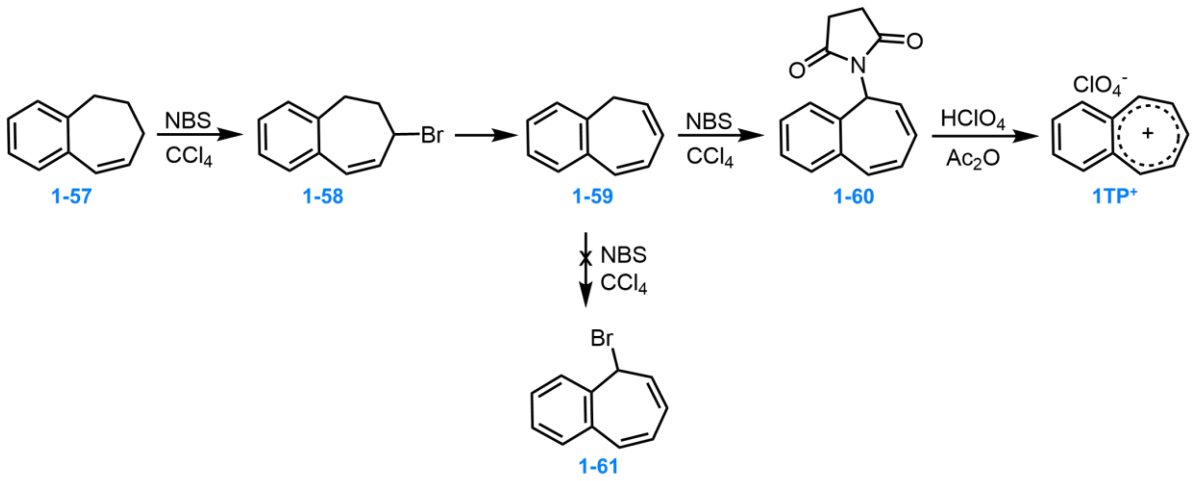

Figure 1.25. Srivastava's synthesis of 1TP$^+$.

Since their first discovery, there have not been many reports on new synthetic methods developed specifically for benzotropyliums (**1TP**$^+$) and naphthotropyliums (**2TP**$^+$). No reports on tropylium acene homologues longer than **2TP**$^+$ have been made either, except in 1989, when **2TP**$^+$ was reported by Komatsu *et al.* as a by-product from the decomposition of a tropylium-incorporated anthracene photodimer (**1-64**) (Figure 1.26).[111]

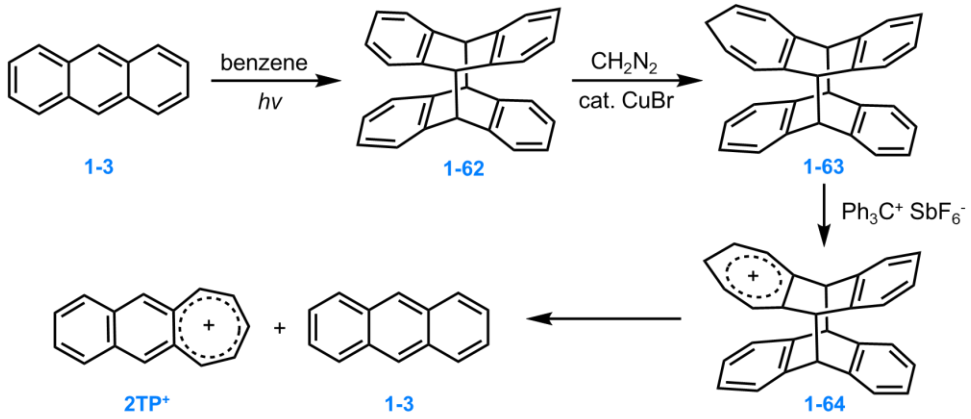

Figure 1.26. Komatsu's synthesis of a tropylium-incorporated anthracene photodimer (**1-64**), which decomposes to form anthracene (**1-3**) and **2TP**$^+$.

In this reaction, a solution of anthracene (**1-3**) in deoxygenated benzene was irradiated to generate the anthracene dimer (**1-62**) in high yields. **1-62** was then reacted with diazomethane to generate a **CHT** derivative of the dimer (**1-63**), which was treated with triphenylmethyl hexafluoroantimonate to generate the corresponding cation dimer (**1-64**) as an SbF_6^- salt. Komatsu synthesised this dimer in hopes of investigating the intramolecular electronic interactions between the face-to-face arranged π-systems. However, **1-64** was discovered to be unstable even at room temperature in the dark, and the new species formed were identified by ^{1}H NMR spectroscopy to be a mixture of anthracene and **2TP**$^+$. Since **2TP**$^+$ was not the intended research target, it was not investigated further.

While tropylium tetrafluoroborate is a widely used reagent and a useful precursor to numerous compounds such as azulenes,[112] substituted cycloheptatrienes[113] and hydroxyl barbaralanes,[114] tropylium acenes have found fewer applications. In 2006, the pK_{R+} values, NMR chemical shifts and reduction potentials of **1TP**$^+$ and **2TP**$^+$ were measured and used as reference compounds for the electrochemical studies of novel areno-annulated tropylium ions synthesised by Naya *et al.* (Figure 1.27).[115]

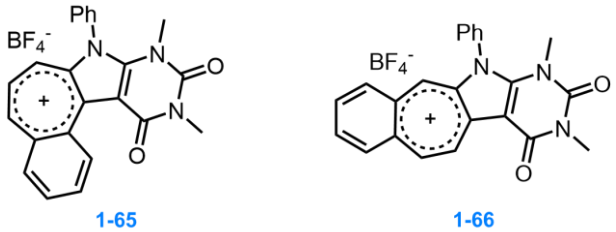

Figure 1.27. Novel areno-annulated tropylium ions synthesised by Naya.

More recently, **1TP**$^+$ was used as a precursor for the synthesis of a vinylheptafulvene compound (**1-69**) by Skov *et al*. (**Figure 1.28**).[116] **1-69** was used in the investigation of a novel dihydroazulene-vinylheptafulvene (**DHA – VHF**) photochromic system, which has been exploited for light-inducing conductance switching in molecular electronic devices.[117] However, it was discovered that when the **CHT** group on a conventional **VHF** structure is replaced by a benzo-**CHT** group to form **1-69**, the **VHF** (**1-69**) is unable to convert to the corresponding DHA (**1-70**).

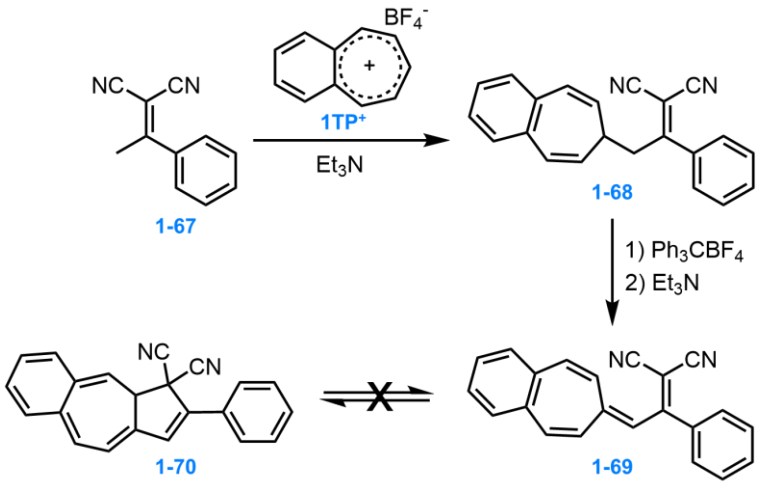

Figure 1.28. A VHF with a benzo-CHT group (1-69) does not convert to the corresponding DHA (1-70).

2. Project Aims

Over the years, polycyclic aromatic hydrocarbons (**PAH**s) have been exploited as components of organic molecular electronic devices. Acenes, namely tetracene and pentacene have been used in photovoltaics due to their ability to undergo singlet fission. Studies have been made to tune the electronic properties of these materials by introducing functional groups,[62] extending the conjugated system[118] and twisting the aromatic surface.[119] However, no reports to date have taken advantage of aromatic cations based on seven-membered rings (i.e. fused tropylium rings) in functional **PAH**s, making this a fundamental area of organic materials that has not yet been explored.

Tropylium ions (**TP**$^+$) possess unique characteristics which set them apart from common organic motifs. Due to their aromaticity, they exhibit remarkable thermodynamic and kinetic stabilities relative to traditional carbocations, rendering them bench stable.[71] On the other hand, **TP**$^+$ are considerably more redox-active than neutral aromatics due to their ability to stabilise charge and to undergo more facile electrochemical reduction. Moreover, **TP**$^+$ exhibit enhanced dispersion of their positive charges over other cations such as ammoniums and phosphoniums, making them better charge carriers. Nonetheless, despite these unique and desirable properties, **TP**$^+$ have not been well explored in the design of functional materials.

This project therefore aims to develop synthetic methods for a series of novel tropylium acenes, so that their electronic and photophysical properties can be investigated experimentally. The ultimate goal would be to evaluate these materials as singlet fission chromophores for photovoltaics. It is hypothesised that acenes' well-known ability to undergo singlet fission, coupled with **TP**$^+$'s high carrier mobility, creates great potential for tropylium acenes to become a novel class of singlet fission materials for photovoltaics.

From previous quantum chemical modelling and DFT calculations carried out by Dr Paul McGonigal and Dr Rubia Ayub, attractive tropylium acene targets with desirable singlet and triplet energies to allow for singlet fission have been identified. As shown in Figure 2.1, structures **2-1** and **2-2** have been predicted to satisfy the fundamental singlet fission requirement of $2\ E(T_1) \leq E(S_1)$.

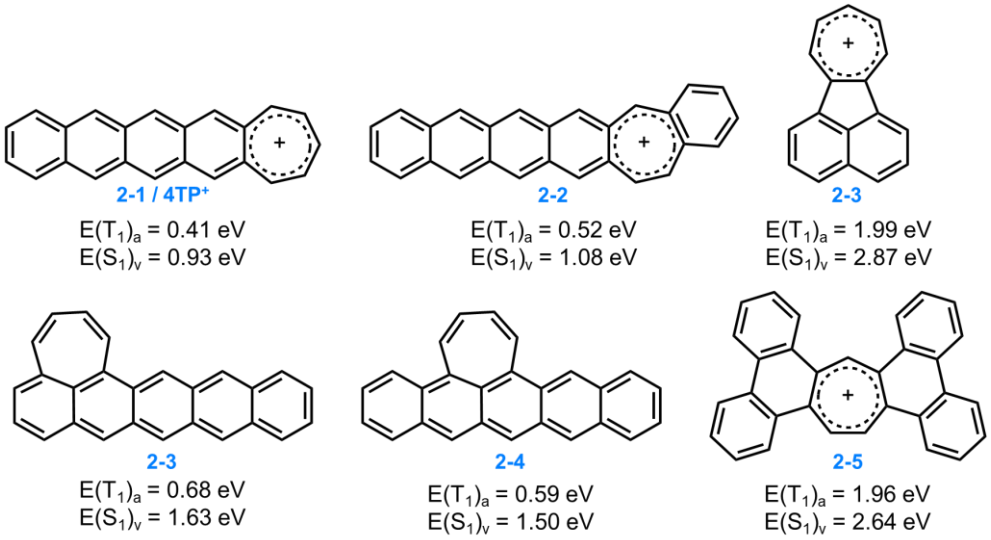

Figure 2.1. Adiabatic triplet and vertically excited singlet energies of compounds **2-1** to **2-6** at M06-2X and TD-M06-2X/6-311G+(d,p).

This report outlines the approach taken in hopes of synthesising tetracene tropylium (**4TP**$^{+}$). The aim would be to develop a synthetic pathway which can be applied to the parent tetracene (**1-4**) which is already commercially available, and generate the corresponding tropylium acene.

3. Results and discussion

3.1 Synthesis of 1TP$^+$ via Buchner ring expansion

Although the synthesis of benzoropylium (**1TP$^+$**) has already been reported, most of the methods often involve using starting materials with a seven-membered ring already attached to a benzene ring, such as benzosuberene[109] (**1-57**) and benzosuberone,[120] both of which are commercially available. These methods therefore would not be applicable for synthesising longer tropylium acenes, as the corresponding starting material required would be much more difficult to access. On this account, attempts were made to design a synthetic method which could be applied to parent acenes to generate the corresponding tropylium acene.

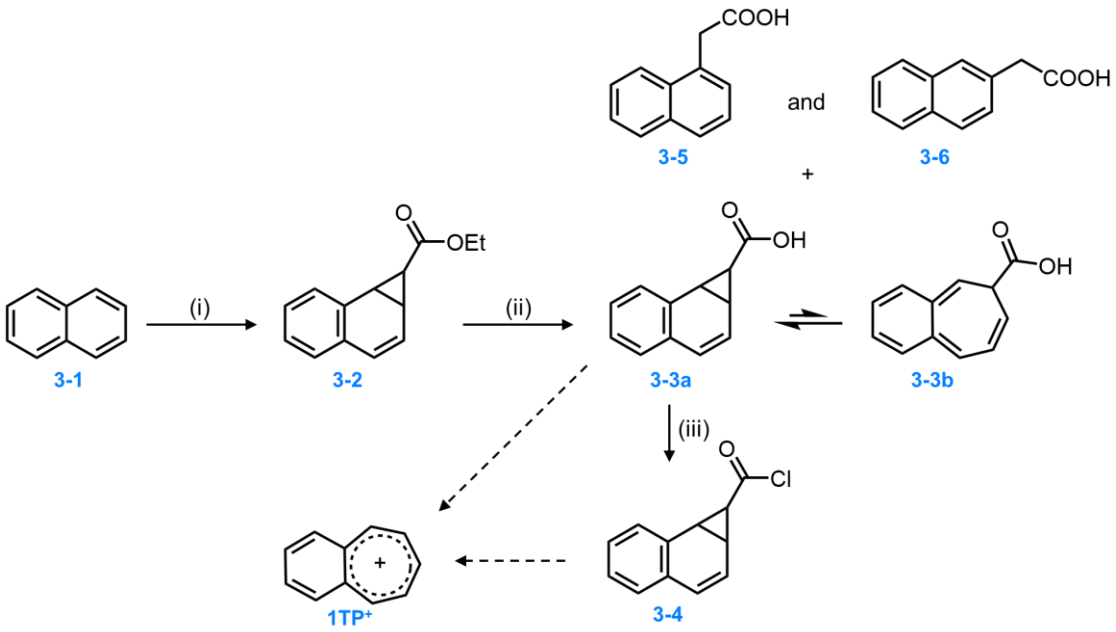

Figure 3.1. Prosed synthetic route for benzotropylium (**1TP$^+$**).[c] Reagents and conditions: (i) ethyl diazoacetate, $Rh_2(CF_3COO)_4$, anhydrous CH_2Cl_2, rt, 2 h; (ii) KOH in H_2O:EtOH, reflux, 30 min; (iii) oxalyl chloride, anhydrous CH_2Cl_2, rt, 16 h.

The first proposed pathway for synthesising **1TP$^+$** involved a classic Buchner ring expansion of naphthalene (**3-1**) to generate a norcaradiene (**3-2**) (Figure 3.1). It was envisioned that if **1TP$^+$** can be successfully generated via this synthetic route, the same method may be applied to longer acenes as well. Following the procedures published by Müller *et al.*,[90] ethyl diazoacetate was reacted with naphthalene with the aid of a rhodium(II) trifluoroacetate dimer

[c] Solid arrows represent successful reactions carried out in this project. Dashed arrows represent proposed reactions that were unsuccessful. Grey arrows represent proposed reactions that have not been carried out.

catalyst, forming ester **3-2**. As **3-2** was reported to decompose partially upon column chromatography, it was directly reacted with KOH solution without purification to generate the carboxylic acid **3-3** via ester hydrolysis. Purification of the crude residue by column chromatography was found to be challenging as it contained a mixture of naphthaleneacetic acid isomers (**3-5** and **3-6**) which had very similar polarities to the product (**3-3**) and hence were difficult to separate. Pure **3-3** was therefore obtained from column chromatography with only 12% yield. Attempts were made to purify the remaining impure mixture by recrystallisation but were unsuccessful. More work is therefore needed to seek an alternative way to purify the mixture in order to maximise the yield of the reaction.

In the ^{1}H NMR spectrum of **3-3** (Figure 3.2), two olefinic (H_4 and H_5), two allylic (H_2 and H_3) and one alkyl (H_1) proton environments were observed, indicating the norcaradiene (**NCD**) tautomer was formed exclusively in this reaction. If any **CHT** tautomers were present, more olefin peaks would be observed in the ^{1}H NMR spectrum. This observation agrees with Hoffmann's postulate,[96] as a carboxylic group at the C_1 position is a π-acceptor which favours the **NCD** tautomer (see Section 1.3.1.1). The **NCD** tautomer also benefits from aromatic stabilisation by having a complete Clar sextet, which the **CHT** tautomer doesn't.

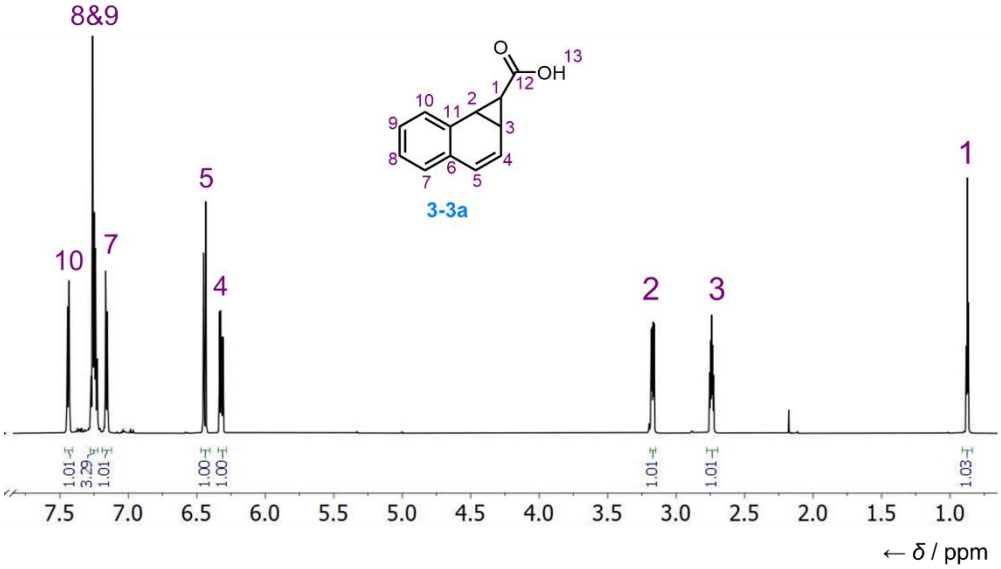

Figure 3.2. ^{1}H NMR (500 MHz, $CDCl_3$, 298 K) spectrum of **3-3a**, which indicates the **NCD** tautomer.

The carboxylic acid **3-3** was then reacted with thionyl chloride in hopes of forming acyl chloride **3-4**, but the reaction was unsuccessful and generated mostly naphthalene, as proven by the crude ^{1}H spectrum. Oxalyl chloride was used as an alternative reagent, which

successfully generated relatively pure **3-4** quantitatively. As **3-4** is extremely sensitive to moisture and can revert back to **3-3** easily, purification by column chromatography was not viable as there would be too much exposure to moisture. The product was therefore stored under nitrogen and used in subsequent reactions without further purification.

In 1959, Dewar *et al.* prepared a series of tropylium salts (**TP**$^+$ **X**$^-$) via various pathways.[121] A synthetic scheme based on Dewar's work was therefore proposed in hopes of generating **1TP**$^+$ using similar procedures (Figure 3.3). The feasibility of each method was considered in terms of material availability, safety and predicted yield.

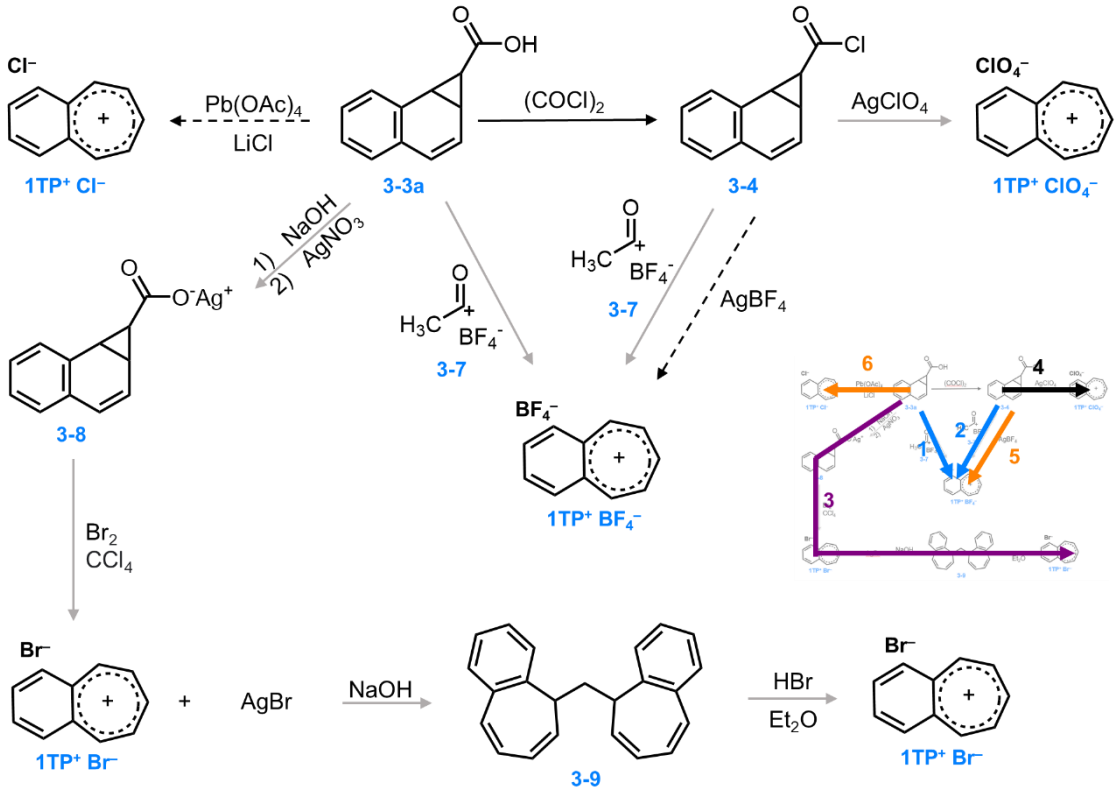

Figure 3.3. Proposed pathways of converting **3-3a** or **3-4** to various benzotropylium salts (**1TP**$^+$ **X**$^-$). A small legend outlining all pathways is provided for clarity. Routes 1-4 are based on procedures reported by Dewar *et al.*[121] Routes 1 and 2 (blue) both use acetyl tetrafluoroborate (**3-7**) as a regent. Route 3 (purple) is a Hunsdiecker-like reaction. Route 4 (black) uses silver perchlorate. Routes 5 and 6 (orange) are methods attempted during this project but were unsuccessful.

Firstly, Dewar reported the successful generation of **TP**$^+$ **BF**$_4^-$ by reacting the carboxylic acid precursor and the acid chloride precursor with acetyl tetrafluoroborate (**3-7**), achieving a 93% and 41% yield respectively. It was therefore proposed that reacting **3-3a** or **3-4** with **3-7** should both lead to the formation of **1TP**$^+$ **BF**$_4^-$ (routes 1 & 2 in Figure 3.3). Upon further research, however, it was discovered that **3-7** is a very difficult reagent to prepare. **3-7** was first reported

by Seel in 1943, who reacted acetyl fluoride with boron trifluoride in liquid sulfur dioxide at low temperature.[122] Acetyl fluoride is also not a readily available reagent and needs to be generated by reacting acetyl chloride with potassium fluoride at low temperature.[123] As these reactions all require the handling of various corrosive gasses at low temperatures, special apparatus would be required to carry out the experiments. It was therefore concluded that the method is not practical for this project.

On the other hand, Dewar also generated **TP$^+$ Br$^-$** by carrying out a Hunsdiecker reaction where the acyl group is removed via decarboxylation (route 3 in Figure 3.3)[d].[124] The carboxylic acid precursor was first neutralised by sodium hydroxide and converted into a silver carboxylate salt (**3-8**) by reacting with silver nitrate. The silver salt was then reacted with bromine in refluxing carbon tetrachloride, during which carbon dioxide gas was liberated. After filtration, the yellow precipitate was found to be a mixture of insoluble silver bromide and **TP$^+$ Br$^-$**. Attempts were made to isolate **TP$^+$ Br$^-$** by extracting with water or ethanol, but only a small amount was recovered. The mixture was therefore vigorously agitated with aqueous sodium hydroxide, converting **TP$^+$ Br$^-$** into biscycloheptatrienyl ether, which was extracted with diethyl ether and converted back to **TP$^+$ Br$^-$** by reacting with hydrogen bromide**.** These extra steps required to isolate the product meant that the yield was significantly lowered to less than 5%. Therefore even though a Hunsdiecker reaction seemed feasible for generating **1TP$^+$ Br$^-$** due to all the reagents being readily available and relatively safe, based on the already low yield in synthesising the carboxylic acid precursor **3-3a** obtained in this project as previously mentioned, it may be difficult to isolate the desired product in a meaningful quantity.

Dewar also reported the generation of **TP$^+$ ClO$_4^-$** by treating the acid chloride precursor with silver perchlorate, at a 28% yield. However, the use of perchlorate salts in current days has been discouraged due to safety concerns regarding their explosiveness. Silver tetrafluoroborate was therefore used as an alternative in this project, in hopes of generating **TP$^+$ BF$_4^-$** from **3-4**. Indeed, a precipitate was formed, suggesting the acid chloride group had reacted due to the possible formation of silver chloride and/or **TP$^+$ BF$_4^-$**. However, the reaction appeared to be unsuccessful as the ^{1}H NMR spectrum of the filtrate showed that most of the starting material remained unreacted. Any newly formed products were unable to be isolated due to the low conversion and small reaction scale.

[d] Route 3 in Figure 3.3 is the proposed pathway for **1TP$^+$**. Dewar's synthesis of **TP$^+$** was the same as this pathway, only without the extra benzene ring on each structure.

After failing to apply Dewar's procedures, attempts were made to generate **1TP$^+$ Cl$^-$** from **3-3a** via a Kochi reaction, which involved a decarboxylation reaction using lead(IV) acetate and lithium chloride.[125] The reaction again appeared to be unsuccessful as preliminary investigations did not return any conclusive results. The crude residue was subjected to column chromatography in order to separate the components as the ^{1}H NMR spectrum of the crude mixture was too complicated to resolve. However, while some fractions showed the formation of new peaks in the upper aromatic region, which suggested the possible formation of a cation, the peaks did not match the ^{1}H NMR chemical shifts of **1TP$^+$** from literature.[116]

The probability of success of this synthetic route was review after multiple failures in generating **1TP$^+$**. If this method were applied to longer acenes, an increasing number of regioisomers would form during the Buchner ring expansion step, resulting in much more challenging purification even in the first step. Coupled with the difficulties encountered in the final step, it was decided that an alternative route should be sought.

3.2 Synthesis of 2TP$^+$ via Birch reduction

The second proposed approach involved the Birch reduction of anthracene (**3-10**) to form a tetra-alkene product (**3-11**),[126] followed by a Simmons-Smith cyclopropanation of one of the alkenes to form regioisomers **3-12** and **3-13** (Figure 3.4).[127] **3-12** would then be subjected to aromatisation, via active MnO_2 dehydrogenation,[128] in hopes of generating the norcaradiene **3-14a**, which would be in an equilibrium with **3-14b**. The **CHT** tautomer **3-14b** is expected to be heavily favoured due to the Clar sextet formed. It may be converted to **2TP$^+$** directly in the presence of the MnO_2 oxidant, or by adding trityl salts.[74]

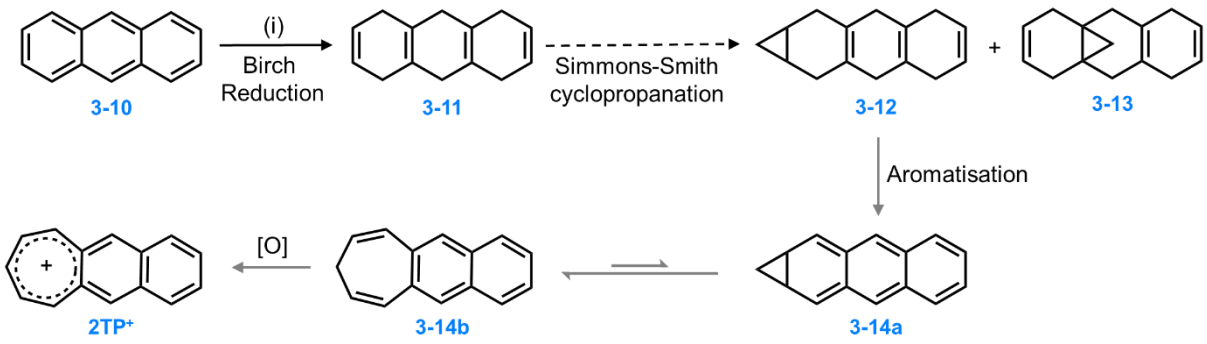

Figure 3.4. Proposed synthetic route for naphthotropylium (**2TP$^+$**). Reagents and conditions: (i) Na, $NH_{3\,(l)}$, −78 °C, 16 h.

To carry out the Birch reduction, ammonia gas was first condensed to a liquid and added to a cooled solution of anthracene (**3-10**) in tetrahydrofuran and ethanol. Sodium metal was then added and a blue layer of solvated electrons was observed. After stirring overnight, the reaction was allowed to warm to room temperature and quenched carefully by the addition of water. The crude product was then obtained via a normal reaction work up.

During the first attempt of the Birch reduction, a number of problems were encountered. Firstly, upon quenching, the remaining sodium and cooled liquid ammonia reacted violently with water at room temperature even with careful, small additions. Secondly, the ^{1}H NMR spectrum of the crude residue showed that the anthracene had not been converted fully to the desired **3-11**, but had only undergone partial Birch reduction to **3-15** (Figure 3.5a). This may be due to the third problem encountered – it was observed that the anthracene solution did not mix well with the solvated electron layer even with vigorous stirring, which may have limited the conversion. Purification of the crude mixture by column chromatography was found to be challenging due to both products having very similar polarities, as well as **3-11** apparently having a very low extinction coefficient. Recrystallization from benzene however, successfully separated pure **3-11** from **3-15** as single crystals, with the structure confirmed by X-ray crystallography (Figure 3.5b).

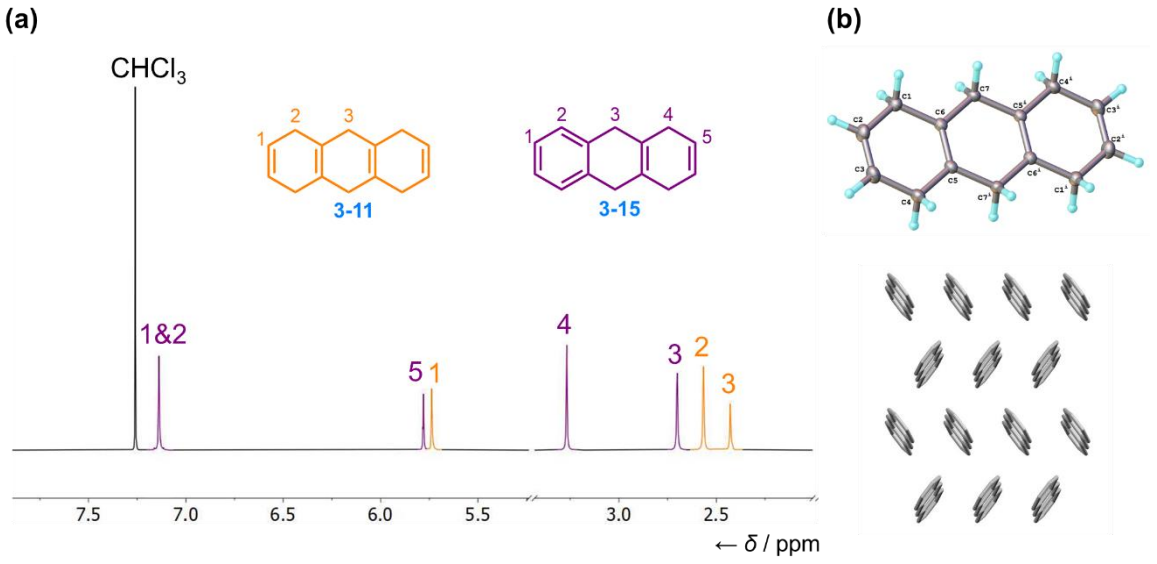

Figure 3.5. (a) ^{1}H NMR (500 MHz, $CDCl_3$, 298 K) spectrum from the first Birch reduction of anthracene, which formed a mixture of the desired product **3-11** (orange peaks) and the partially reduced product **3-15** (purple peaks): δ 7.17 – 7.11 (m, 4H, H1 and H2), 5.75 – 5.73 (m, 2H, H5), 3.28 – 3.25 (m, 4H, H4), 2.70 (s, 4H, H3). (b) The crystal structure of 1,4,5,8,9,10-hexahydroanthracene (**3-11**) and its packing.

Efforts were then made to maximise the conversion of anthracene to **3-11** by varying reaction conditions (Table 3.1). During the second attempt, more care was taken to exclude moisture from the reaction by passing the ammonia gas through a drying tower containing potassium hydroxide before condensing. The reaction time was also increased from 14 h to 24 h, and the ratio between **3-11** and **3-15** increased from 1.16:1 to 2.89:1 (**Figure 3.6**). When the reaction was repeated for the third time, the solvated electrons were first generated in a separate reaction flask by dissolving more equivalents of sodium metal in liquid ammonia, forming a blue solution. The anthracene solution was then added dropwise to the solvated electrons. The ratio of **3-11:3-15**, however, did not improve, which could be due to possible exposure to atmosphere or moisture during handling. During the fourth attempt, more equivalents of sodium metal but half the volume of THF was used, hence tripling the concentration of the reaction mixture. A slightly different approach was also used to work up the reaction – the reaction mixture was allowed to warm up to room temperature with vigorous stirring until all the ammonia had evaporated, which took approximately 30 minutes. A condenser was fitted to the reaction flask to prevent spillage from evaporation. It was observed that as the reaction mixture started warming up, the solvated electron mixed in better with the anthracene solution and the whole reaction mixture became blue instead of two separate layers. The better mixing was believed to have increased conversion. As the entire reaction mixture became white, which suggested that all solvated electrons have reacted or quenched themselves, water was added, during which effervescence was not observed. The usual separation and purification were subsequently carried out, and it was discovered that a 95% conversion was achieved and successfully generated **3-11** at 81% yield.

Table 3.1. Summary of conditions screened for the Birch reduction of anthracene to form **3-11**.

	Na added / equiv. wrt antracene	**Reaction time / h**	**Volume of THF used / mL**	**Integration of 3-11 : 3-15**	**Other comments**
1	20	14	80	1.16 : 1	Literature procedures
2	20	24	80	2.89 : 1	More care to exclude moisture
3	30	24	80	2.04 : 1	Electrons generated in separate flask
4	30	24	40	19.8 : 1	Different reaction workup

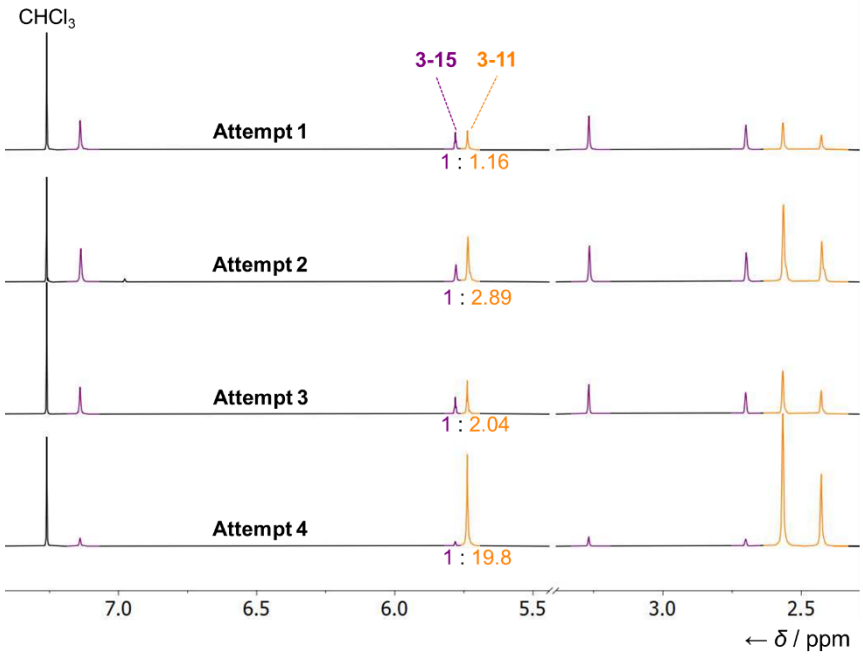

Figure 3.6. Comparison of crude ^{1}H NMR (400 MHz, $CDCl_3$, 298 K) spectra from different attempts of Birch reduction of anthracene. Ratios of the desired product **3-11** (orange) and partially-reduced product **3-13** (purple) are also shown.

Once the Birch reduction of anthracene had been optimised and generated **3-11** in good yield, **3-11** was used to carry out a Simmons-Smith cyclopropanation, which is a chelotropic reaction involving the reaction of diiodomethane and a zinc-copper couple with an alkene to form a cyclopropane via the formation of an organozinc carbenoid. Such a reaction with substrate **3-11** has not been reported in literature. The first attempt of the reaction was carried out following procedures reported by Friedrich *et al.* from their study on the regioselectivity and solvent effects on the mono-cyclopropanation of alkadienes.[129] Friedrich realised that the organozinc intermediate is electrophilic but rather sterically hindered; using a non-coordinating solvent therefore causes the intermediate to preferably react with the less hindered olefin, hence generating the less hindered cyclopropane isomer. After screening the cyclopropanation of limonene with various solvents, Friedrich discovered that 1,2-dichloroethane was the best solvent for alkadienes as the less sterically hindered structure was the major isomer. These conditions were therefore used in this project, in hopes of generating the less hindered **3-12** as the desirable major product. During the reaction, the reactant **3-11**, zinc dust and copper(I) chloride were all dissolved in 1,2-dichloroethane, with a catalytic amount of acetyl chloride added to promote the reaction.[130] The zinc-copper couple was generated *in situ*, and the reaction mixture was heated at 50 °C for 24 h. However, upon preliminary investigations it was

concluded that the reaction was unsuccessful. The ^{1}H NMR spectrum of the crude residue showed a mixture of products, which were formed by the oxidation of **3-11** (Figure 3.7). As the reaction was carried out in an inert atmosphere, the formation of oxidised product could be explained by the starting material reacting with oxygen dissolved in the solvent.

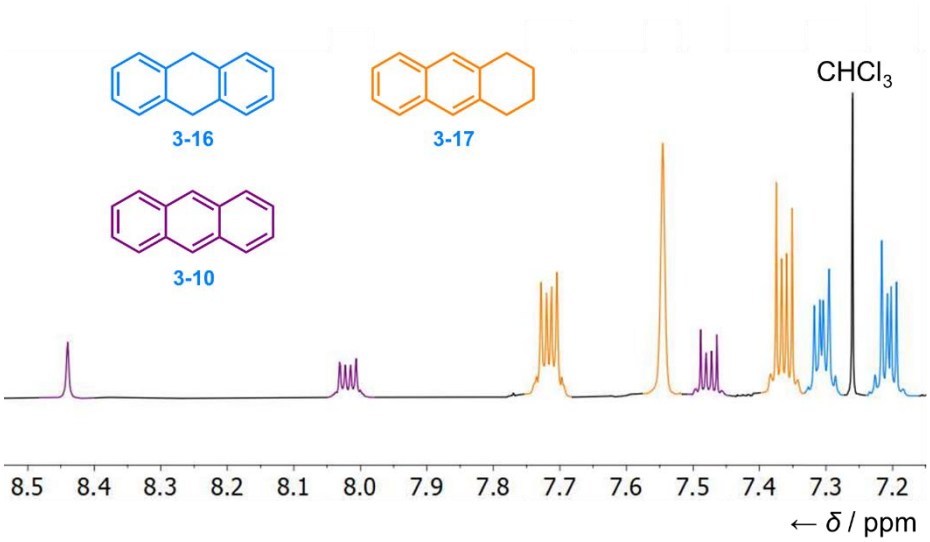

Figure 3.7. The aromatic region of the partial ^{1}H NMR (500 MHz, $CDCl_3$, 298 K) spectrum of the crude mixture from the first attempt of the Simmons-Smith cyclopropanation of **3-11**. The peaks of different products formed are shown in different colours.

The second attempt at cyclopropanating **3-11** followed reaction conditions reported by Gensler, who synthesised norcarane (**3-19**) from 1,4-cyclohexadiene (**3-18**), which were both similar structures to the target reaction (Figure 3.8).[127] When this reaction was carried out, all solvents used were first degassed via three freeze-pump-thaw cycles in order to remove all oxygen present and prevent the formation of oxidised products. Zinc dust and copper(I) chloride were suspended in degassed, anhydrous diethyl ether and refluxed for 1.5 h to generate the zin-copper couple. Compound **3-11** and diiodomethane was subsequently added, and the reaction mixture was refluxed for a further 21 h. The reaction was again unsuccessful as the ^{1}H NMR spectrum of the crude mixture showed that most starting material had remained unreacted, with only trace amounts of oxidised product **3-15** present.

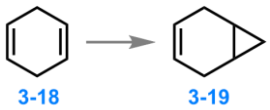

Figure 3.8. Cyclopropanation of 1,4-cyclohexadiene (**3-18**) to norcarane (**3-19**) reported by Gensler.

With the cyclopropanation reactions giving unpromising results, the feasibility of this route was reviewed. If this method is applied to longer acenes, even if the cyclopropanation step were successful, an increasing number of regioisomers with similar polarities would be formed, resulting in extremely challenging purification. As the following aromatisation step proposed is unprecedented as well, it was decided that an alternative route should be sought.

3.3 Synthesis of 3TP$^+$ via Knoevenagel condensation

The third approach taken to synthesise tropylium acenes was based on the work of Heilbronner *et al.* (mentioned in Section 1.3.2) from the 1950s,[108,120] which involves a Knoevenagel condensation of acene dialdehydes (**3-22**) with diethyl-1,3-dicarboxylate (**3-23**) to form **3-24**, followed by a decarboxylative hydrolysis to remove the two ester groups (Figure 3.9). The tropones (**3-25**) may then be reduced by lithium aluminium hydride to form the alcohols (**3-26**), which may form the corresponding tropylium acenes (**2TP$^+$/3TP$^+$**) upon treatment with acid.

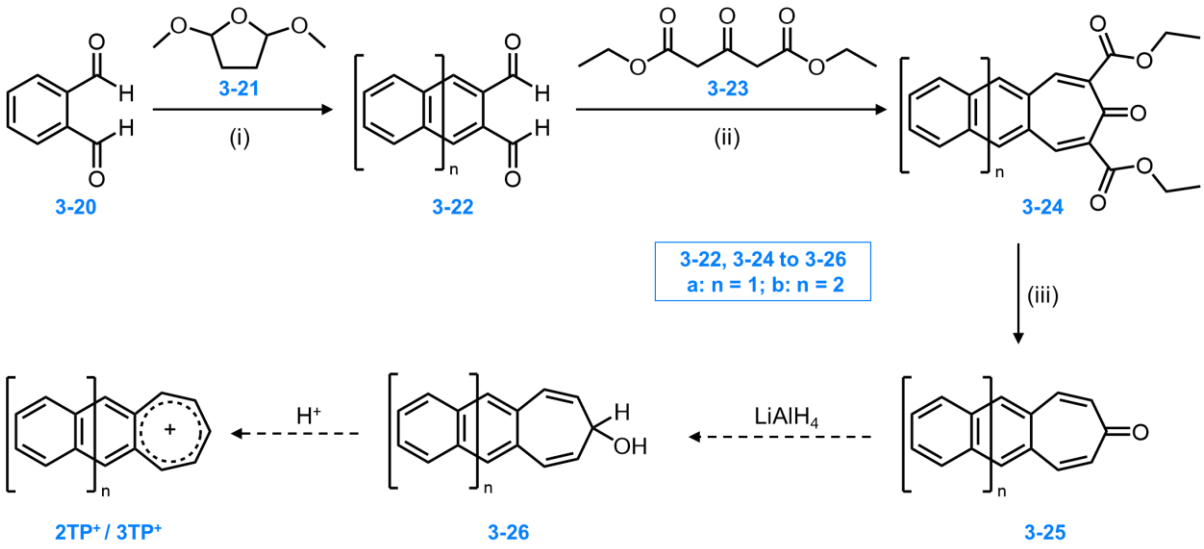

Figure 3.9. Proposed synthetic route for **2TP$^+$** and **3TP$^+$** based on the work of Heibronner *et al.* Reagent and conditions: (i) 100% acetic acid, water, piperidine, reflux, 24 h. (ii) Piperidine acetate, piperidine, toluene, reflux, 2h. (iii) 5% KOH in methanol, reflux, 4 h.

Although Heilbronner reported the reaction of **3-22a** and **3-23** to form **3-24a**, it was unclear how they obtained the starting material **3-22a**. At the present time, as **3-22a** and **3-22b** are too expensive to purchase, a method is therefore needed to obtain a series of acene dialdehydes. Most reports on the synthesis of acene dialdehydes involved cumbersome multistep syntheses.[131,132] Fortunately, a method developed Malloui and Lepage provided a convenient,

one-step synthesis to access **3-22a**, **3-22b**, and tetracene dialdehyde from commercially available starting materials. Their reaction involved the condensation of *o*-phthaldialdehyde (**3-20**) and 1,4-dioxobutane – which was generated *in situ* by the hydrolysis of 2,5-dimethoxytetrahydrofuran (**3-21**), in acetic acid and a few drops of piperidine. The ratio of products was controlled by changing the number of equivalents of **3-21** used, as the dialdehyde products formed can react further to generate longer acene dialdehydes. The reaction was heated under reflux overnight, and worked up by washing the crude residue with hydrochloric acid, water, methanol and diethyl ether. The products were then isolated by sublimation at different temperatures under vacuum, obtaining **3-22a** and **3-22b** at 20% and 17% yield respectively.

After multiple repeats, it was discovered that even when the procedures reported for **3-22b** was used, a significant amount of **3-22a** was still present in the crude mixture. Attempts to drive the reaction further with longer heating times generated a deep red solid, insoluble in any solvent, which was later proved to be tetracene dialdehyde by mass spectrometry.

Efforts were made to separate **3-22a** and **3-22b**, which proved to be extremely challenging. Washing the crude residue with solvents mentioned above produced a red solid which was found to be relatively pure **3-22b**, with only 5% yield. Analysis of the washings revealed a significant amount of dissolved product, due to **3-22a** being completely soluble and **3-22b** being partially soluble in diethyl ether. The solvent was therefore removed *in vacuo* and the remaining residue was subjected to sublimation. However, due to the lack of proper sublimation set up, the product was not obtained in significant amounts.

The crude residue from the next attempt of the reaction was subjected to purification by column chromatography, eluting with hexane and ethyl acetate in hopes of recovering the products at higher yields. Due to their similar polarities, however, the products remained very difficult to separate even with a long column and very shallow solvent gradient.

With conventional methods failing to separate **3-22a** and **3-22b** efficiently, centrifugation was considered in hopes of purifying the crude mixture without losing too much product from washing with organic solvents. After repeating the reaction, the crude residue was first washed with hydrochloric acid and water and filtered through a glass sintered funnel. The filtered solid was then transferred to a centrifuge tube and suspended in methanol. The suspension was centrifuged for 10 minutes, after which the solid was discovered to have sedimented at the

bottom of the tube. The clear, yellow supernatant was decanted the solid remaining was resuspended in diethyl ether and centrifuged again. After decanting the supernatant, the solid residue was dried *in vacuo* and the resulting red solid was confirmed by ^{1}H NMR spectroscopy to be pure **3-22b**. By purifying the crude residue through centrifugation, the yield was increased to 18%, which was comparable to yield quoted in literature.[133]

On the other hand, it was discovered that **3-22b** is unstable and decomposes when exposed to oxygen and light, possible converting to the corresponding endoperoxide or quinone (**Figure 3.10**). The material was therefore always stored in the dark at low temperature to prevent decomposition.

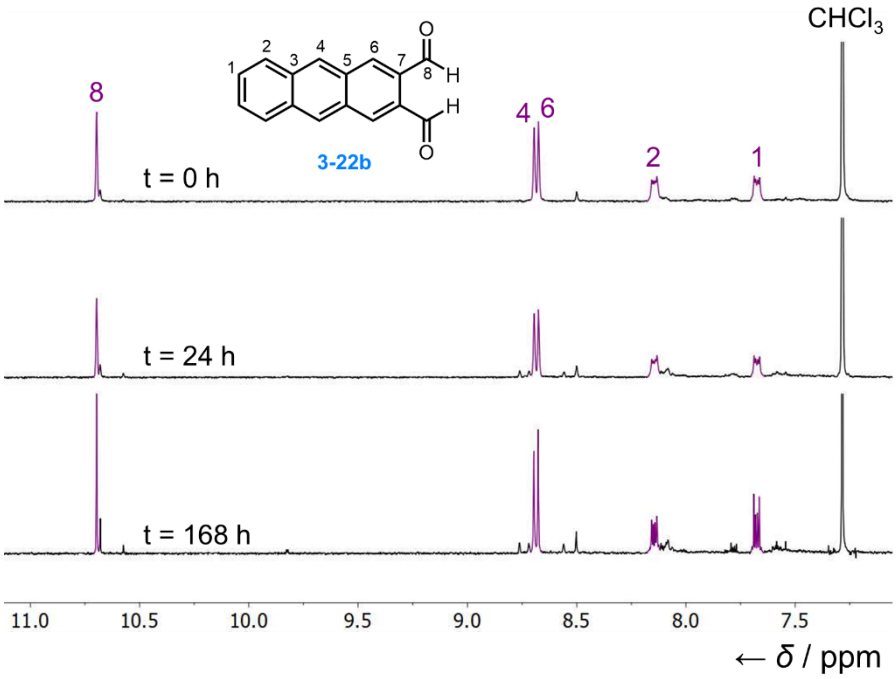

Figure 3.10. Comparison of ^{1}H NMR (500 MHz, $CDCl_3$, 298 K) spectra of the same sample of **3-22b** (peaks highlighted in purple) at t = 0 h, 24 h and 168 h, showing that **3-22b** started to decompose as time increased, and new peaks started to emerge on the base line.

Once a relatively efficient method of purifying **3-22b** has been found, the pure material was used in subsequent reactions. Following Heilbronner's procedures and reacting **3-22b** with **3-23** via a Knoevenagel condensation in the presence of diethylamine was unsuccessful,[108] as proven by the crude ^{1}H NMR spectrum. Piperidine and glacial acetic acid were then used in the following attempts at the reaction, in hopes of generating piperidine acetate *in situ* as an alternative base. This method was inspired by the work of Troschutz *et al.*, who synthesised a similar diester-tropone (**3-28**) via a Knoevenagel condensation (Figure 3.11).[134]

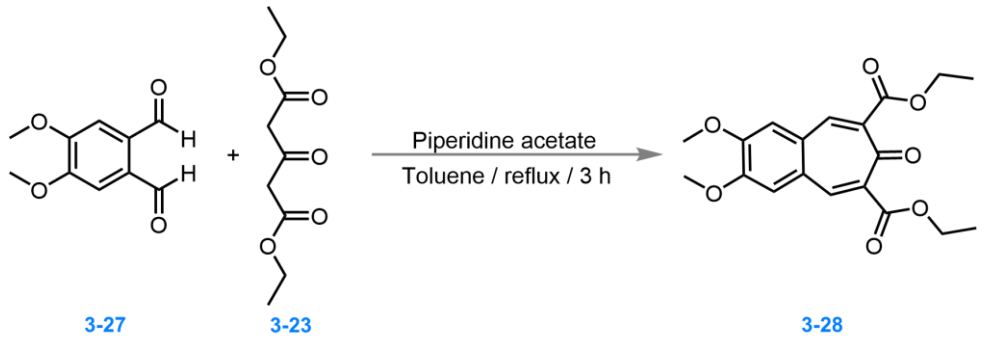

Figure 3.11. Troschutz's method for synthesising a diester-tropone (**3-22**) via a Knoevenagel condensation, which had a similar structure to that of **3-24b**.

The first attempt at using piperidine acetate as an alternative base was unsuccessful as the desired product was not visible in the crude ^{1}H NMR spectrum. The major component in the crude residue was found to have a peak with a very high chemical shift at 13.2 ppm, suggesting the presence of a carboxylic acid group. After repeating the reaction, the ^{1}H NMR spectrum of the crude residue showed that the desired product **3-24b** and the major impurity were present in a 1:1 ratio. The crude material was therefore subjected to column chromatography in hopes of isolating **3-24b**. By trialling different column conditions, it was discovered that a slow gradient up to 10% methanol in dichloromethane worked best at separating different components. Nevertheless, the fraction containing the product was still found to be impure. However, the major impurity (**3-29**) was successfully isolated and crystallised (Figure 3.12). **3-29** was found to be a tricyclic structure which had formed from the dialdehyde (**3-22b**) reacting with two molecules of diethyl-1,3-acetonedicarboxylate (**3-23**). The crystal structure of **3-29** revealed that two intramolecular hydrogen bonds present between each of the hydroxyl protons (H_{11}) and two carbonyl oxygens (O_{12}), which explained the high chemical shifts of the hydroxyl protons.

As the formation of **3-29** is likely due to an excess of **3-23** in the reaction, it was made sure that only one equivalent of **3-23** was used in subsequent attempts at the reaction in order to maximise conversion to the desired product **3-24b**. ^{1}H NMR spectroscopy on the crude residue showed that the conversion had indeed improved. Column chromatography was then carried out again, this time using a longer column and an extremely slow gradient between 5% and 10% methanol to isolate the product, but to no avail. When the column was observed under UV light, it was discovered that three different components had co-eluted with the desired product. A different method therefore needed to be sought in order to purify the product.

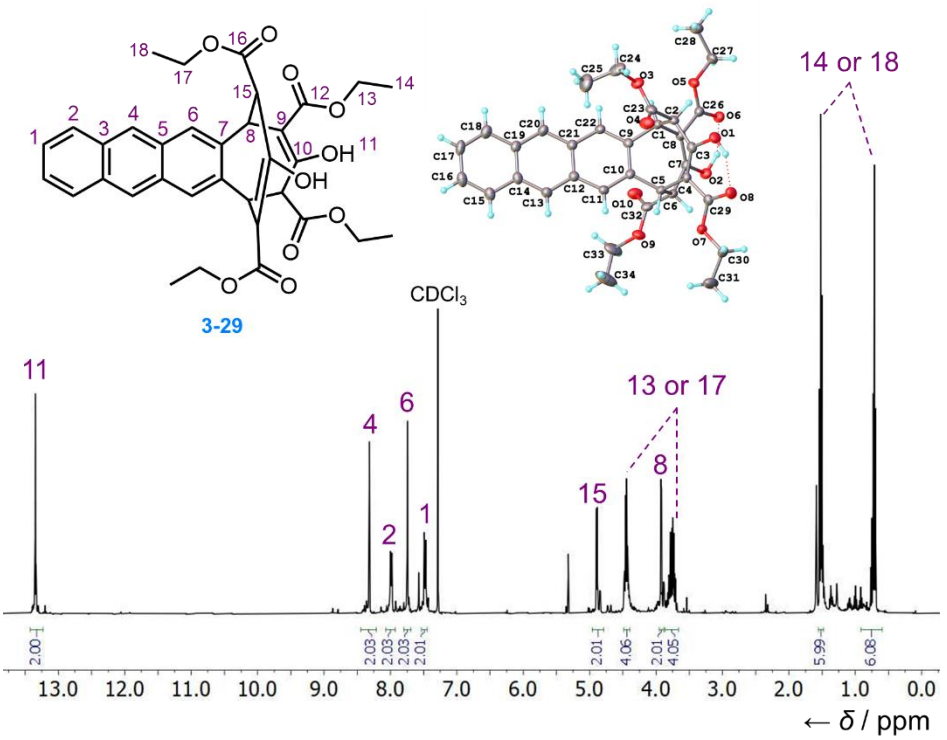

Figure 3.12. ^{1}H NMR (400 MHz, $CDCl_3$, 298 K) spectrum and crystal structure of the tricyclic by-product (**3-29**), formed from dialdehyde **3-22b** reacting with excess **3-23**.

Inspired by the procedures from the previous step, attempts were made to purify **3-24b** from centrifugation, which worked well. The solvent in the impure column fraction was first removed *in vacuo*. The residue was then washed with diethyl ether repeatedly to completely remove any remaining methanol or dichloromethane. Centrifuging the suspension of the residue in toluene generated an insoluble red solid that was proved to be the pure desired product, with a yield of 30%. Crystallisation of the product in toluene generated the oxidised quinone derivative of **3-24b**, but nevertheless proved the success of the Knoevenagel condensation (Figure 3.13a).

Several repeats of the reaction were carried out to determine whether the crude residue could be purified directly without subjected to column chromatography. A UV-Vis spectrum of **3-24b** was also obtained in order to determine the wavelength at which **3-24b** absorbs the most strongly (Figure 3.13b), so that the detector on the chromatography instrument can be adjusted to detect **3-24b** most efficiently. However, it was discovered that changing the detector wavelength did not allow for better separation by column chromatography. Centrifuging the crude residue directly did not purify the product either, meaning it must first undergo column chromatography.

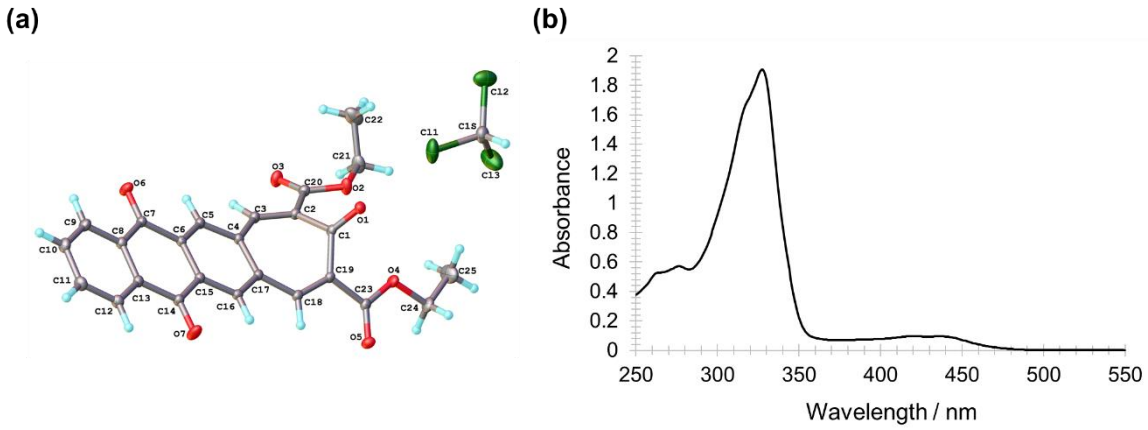

Figure 3.13. (a) Crystal structure of oxidised **3-24b**, formed as a chloroform monosolvate. (b) UV-Vis spectrum of 80 mM **3-24b** in dichloromethane, showing λ_{max} = 330 nm.

Pure **3-24b** was subsequently refluxed with 5% potassium hydroxide in methanol in hopes of forming tropone **3-25b** via removal of the ester groups by decarboxylative hydrolysis. The yield for this reaction was extremely low, possibly due to the ester groups only being partially hydrolysed into carboxylate ions, which remained in the aqueous layer during workup. The reaction was repeated in attempt to improve the yield by increasing reaction times, as well as using 20% potassium hydroxide instead of 5%. However, neither repeat seemed to have improved the yield.

Column chromatography was again unable to fully purify **3-25b**. The ^{1}H NMR spectrum showed significant amounts of impurities in the alkyl region, most likely from grease which is present in solvents. This could be due to the small amounts of reactants, but large volumes of solvents used. Nevertheless, the regions showing product peaks were pure, allowing ^{13}C and 2D NMR spectra to be obtained, thereby confirming the formation of **3-25b**. As the crude yield was so low it was not possible to purify the product by centrifuging either. In order to improve column conditions, a UV-Vis spectrum was obtained in attempt to determine the excitation wavelength of **3-25b**. However, as the sample subjected to UV-Vis spectroscopy was not fully pure in the first place, it was not possible to definitively determine the λ_{max} for **3-25b**. Nevertheless, the original NMR solution was pure enough to allow a single crystal to form. The structure of **3-25b** was therefore confirmed by X-ray crystallography. A stability study was also carried out by obtaining ^{1}H NMR spectra of the same solution of **3-25b** at different time points (Figure 3.14.). Over the course of 10 days, it was discovered that the solution of **3-25b** oxidised to its quinone derivative (**3-30**) when left under ambient light.

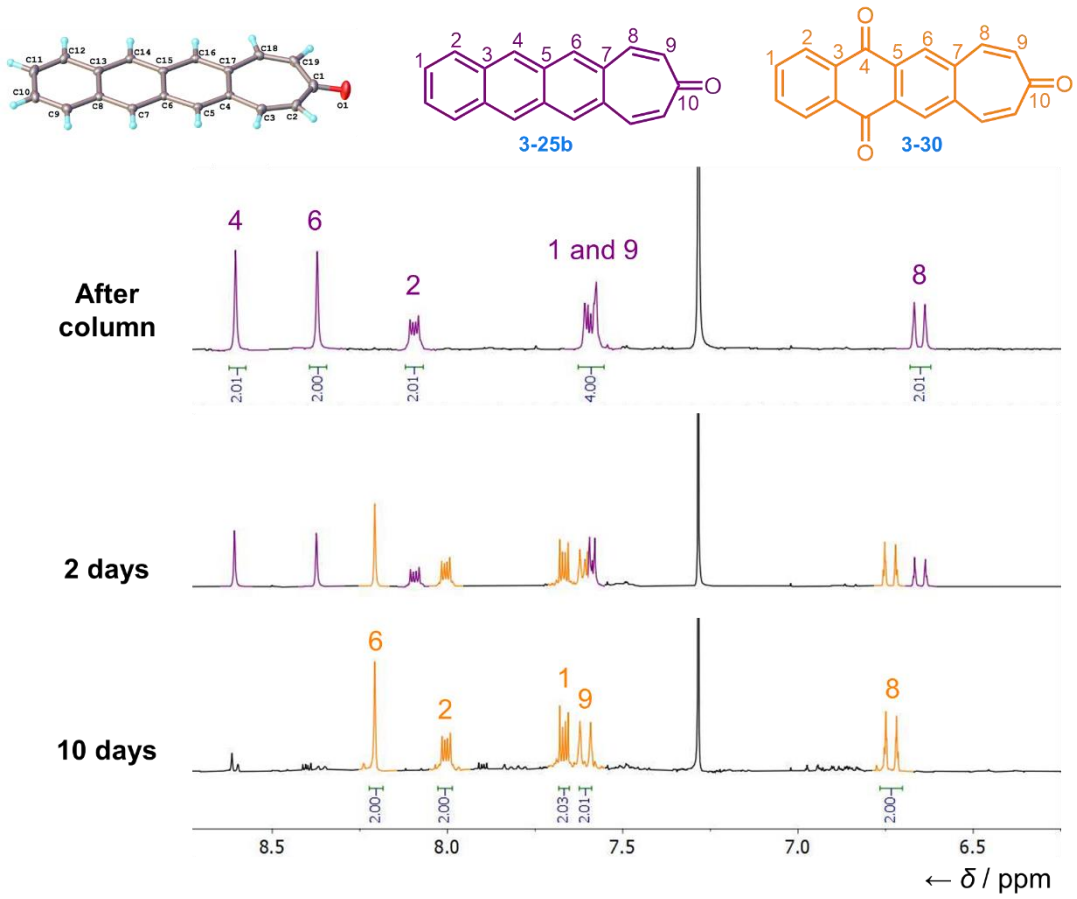

Figure 3.14. Crystal structure of **3-25b**, and a series of ^{1}H NMR (400 MHz, $CDCl_3$, 298 K) spectra showing the oxidation of **3-25b** (purple peaks) to form quinone **3-30** (orange peaks). The time points shown are (top) immediately after being purified by column chromatography; (middle) two days later and (bottom) ten days later.

At the time of writing, attempts to reduce tropone **3-25b** to it corresponding alcohol **3-26b** with lithium aluminium hydride has been unsuccessful, either at room temperature or at 0 °C. Monitoring the reaction and identifying the components in the crude mixture were particularly difficult due to the small scale of the reactions and the low purity of the starting material. More work is needed to increase the yield and fully purify **3-25b**, as well as to develop a method for reducing the ketone group.

Overall, it may be said that the approach of synthesising tropylium acenes via Knoevenagel condensation appears to be the most promising. Although preliminary attempts at reducing **3-25b** to an alcohol have been unsuccessful, this type of reaction is well-documented and there are numerous methods which can be used to carry out the reduction. Once the alcohol is obtained, the tropylium cation should hopefully be easily generated simply by adding an acid.

4. Conclusions and Future Work

In conclusion, various synthetic pathways have been explored in hopes of accessing novel tropylium acene structures, which are predicted to possess desirable singlet and triplet energies ideal for singlet fission and hence the potential to be exploited as materials for organic photovoltaics.

The most promising synthetic route explored involved a Knoevenagel condensation of acene dialdehydes with diethyl-1,3-dicarboxylate, followed by subsequent decarboxylation to generate the corresponding tropone. Attempts to reduce the tropone to the corresponding alcohol have been unsuccessful, a different reduction method is therefore required.

In 2006, Naya *et al.* reported a new method for generating tropylium acenes,[115] which involved a Luche reduction – a selective 1,2-reduction of enones with sodium borohydride, in the presence of cerium(III) chloride (Figure 4.1).[135] Naya reported that although the benzotropylium cation (**1TP**$^+$) can be prepared by reduction of benzotropone with lithium aluminium hydride and subsequent dihydroxylation by perchloric acid, this method did not work as well for naphthotropylium (**2TP**$^+$) due to its instability. They discovered that the reduction of naphthotropone (**4-1**) with sodium borohydride in ethanol, in the presence of cerium(III) chloride and molecular sieves, gave the ethoxide (**4-2**) at 95% yield. The subsequent treatment of **4-2** with perchloric acid in acetic anhydride then afforded **2TP**$^+$ with a 64% yield. Future work therefore hopes to utilise Naya's synthetic procedures to generate **3TP**$^+$, which is believed to be a useful method for the generation of more unstable tropylium ions.

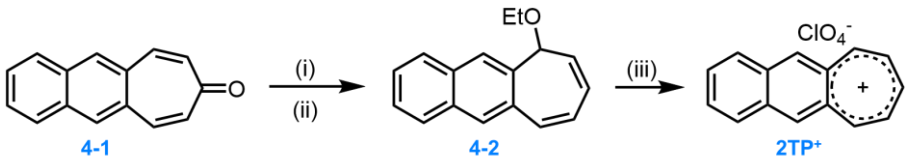

Figure 4.1. Naya's synthesis of **2TP**$^+$ via Luche reduction. Reagents and conditions: (i) $CeCl_3$, EtOH, molecular sieves (0.4 nm), rt, 5 min; (ii) $NaBH_4$, reflux, 5 h; (iii) Ac_2O, $HClO_4$, 0 °C, 20 min.

Although this synthetic route cannot be directly applied to commercially available acenes as initially hoped, it remains the most auspicious attempt at accessing the target molecules. As the synthesis of acene dialdehyde is an iterative reaction, tetracene dialdehyde can in theory be obtained, which could give the target tetracene tropylium (**4TP**$^+$).

On the other hand, an alternative synthetic route based on Komatsu's serendipitous generation of **2TP**$^+$ (Figure 1.26 in Section 1.3.2) could potentially be considered.[111] This method uses the parent acene as a starting material which is preferable, as both tetracene and pentacene are already commercially available. It also takes advantage of acenes' tendency to dimerise. In the case of synthesising **4TP**$^+$, pentacene would be first be irradiated to form a dipentacene butterfly dimer (**4-2**), then reacted with diazomethane to generate a **CHT** derivative (**4-3**) of the dimer (Figure 4.2). Treating **4-3** with triphenylmethyl hexafluoroantimonate should generate the corresponding cation dimer. If **4-4** behaves similarly to its unstable anthracene homologue, it should decompose into a mixture of pentacene and **4TP**$^+$. Alternatively, the dimer may be photolyzed under UV radiation.[136] However, it is also important to note that several problems will be expected. Firstly, acenes are notoriously known for their poor solubility in organic solvents. Since Komatsu had already noted the anthracene dimer had very poor solubility and therefore led to poor yields, it is reasonable to predict that the pentacene homologue, which has an even higher molecular weight, would have much poorer solubility. Secondly, photodimerization of large acenes (tetracene, pentacene and longer) would inevitably generate a mixture of geometric isomers, due to multiple reactive benzene moieties in the acene being able to undergo cycloaddition.[47] These photodimers would have very similar properties and therefore cannot be separated and purified easily.

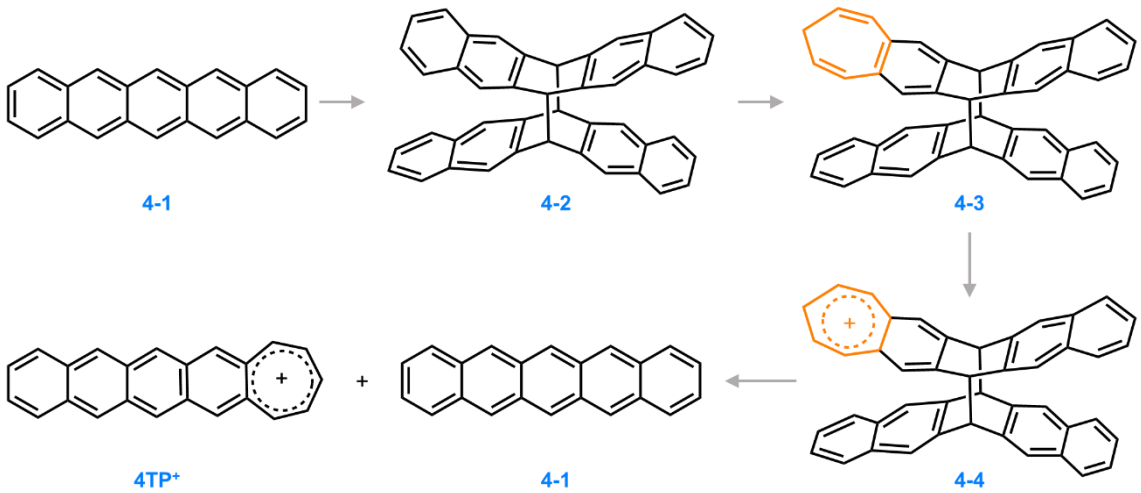

Figure 4.2. Proposed synthetic route for **4TP**$^+$ based on Komatsu's work.

Once the target structures can be synthesised, it is hoped that the compounds can be incorporated into multilayer devices so that investigations on their spin-flip mechanisms and optoelectronic properties can be carried out.

5. Experimental

5.1 General experimental methods

Materials: Unless otherwise stated, all reagents were purchased from commercial suppliers (Sigma-Aldrich, Arcos Organics, Fluorochem or Alfa Aesar) and used without further purification.

Synthesis: Air and moisture-sensitive reactions were carried out under a nitrogen atmosphere using Schlenk techniques. Purification by flash chromatography was carried out using a Teledyne Isco CombiFlash Rf+ system, with pre-packed SiO2 columns as the stationary phase.

Instrumentation and analytical techniques: Analytical TLC was performed on neutral aluminium sheet silica gel plates and visualised under UV irradiation (254 nm). Solution-phase NMR spectra were recorded using a Bruker Advance (III)-400 (^{1}H 400.130 MHz and ^{13}C 100.613 MHz), Varian Inova-500 (^{1}H 500.130 MHz and ^{13}C 125.758 MHz), Varian VNMRS-600 (^{1}H 600.130 MHz and ^{13}C 150.903 MHz) or a Varian V-NMRS-700 (^{1}H 700.130 MHz and ^{13}C 176.048 MHz) spectrometer, at a constant temperature of 298 K unless otherwise stated. For variable-temperature measurements, operating temperatures were calibrated using an internal calibration solution of MeOH. Chemical shifts are reported in parts per million (ppm) relative to residual non-deuterated solvents [CDCl3: δH = 7.26 or δC = 77.16]. Coupling constants (J) are reported in hertz (Hz). Assignment of the ^{1}H and ^{13}C NMR signals was accomplished by two-dimensional NMR spectroscopy (COSY, HMBC, HSQC, NOESY). NMR spectra were processed using MestReNova version 12.0.4. Data are reported as follows: chemical shift, multiplicity, coupling constants, integration and assignment. Multiplicities are reported as singlet (s), doublet (d), triplet (t), quartet (q) and multiplet (m).

Low-resolution ESI-MS and ASAP-MS were performed using a Waters TQD UPLC ES MS/MS spectrometer and a Waters Xevo QTOF equipped with an Atmospheric Solids Analysis Probe (ASAP), respectively. High resolution ASAP mass spectra were measured using a Waters LCT Premier XE high resolution with ASAP ion source.

Melting points were recorded using a Gallenkamp (Sanyo) apparatus and are uncorrected.

5.2 Synthetic procedures

1a,7b-Dihydro-1H-cyclopropa[a]naphthalene-1-carboxylic acid (3-3)

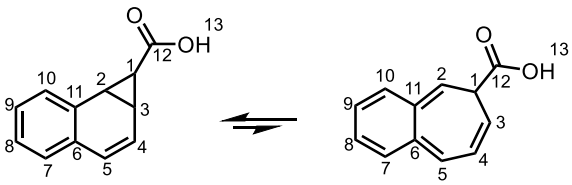

A solution of ethyl diazoacetate (1.14 g, 10.0 mmol, 1 equiv.) in anhydrous CH_2Cl_2 (10 mL) was added to a well-stirred solution of naphthalene (6.43 g, 50.0 mmol, 5 equiv.) and $Rh_2(CF_3COO)_4$ (33 mg, 0.05 mmol, 0.5 mol%) in anhydrous CH_2Cl_2 (100 mL) over 2 h by syringe pump at rt. After addition was completed, stirring was continued for a further 15 min. The solution was concentrated *in vacuo*. KOH solution (1 M in H_2O/EtOH 15:65; 80 mL) was added, and the mixture containing the ester was refluxed for 30 min. After evaporation, the slurry was dissolved in Et_2O (50 mL) and H_2O (50 mL). The aqueous layer was washed with Et_2O (3 × 25 mL). More Et_2O (50 mL) was added and the stirred emulsion was acidified to pH 1 with 1 M aqueous HCl at 0 °C. The aqueous phase was then extracted with Et_2O (3 × 50 mL), and the combined organic phases were washed with brine (2 × 50 mL), dried with $MgSO_4$ and evaporated. The yellow crude residue was purified by column chromatography (Teledyne Isco CombiFlash Rf+ system, 24 g SiO_2, hexane−EtOAc, gradient elution) to yield the title compound as a colourless solid (227 mg, 1.22 mmol, 12%). **^{1}H NMR** (599 MHz, $CDCl_3$) δ 7.44 (dd, J = 7.0, 1.7 Hz, 1H, H_{10}), 7.28 – 7.22 (m, 2H, H_8 and H_9), 7.16 (dd, J = 7.1, 1.9 Hz, 1H, H_7), 6.44 (d, J = 9.5 Hz, 1H, H_5), 6.32 (dd, J = 9.6, 5.0 Hz, 1H, H_4), 3.17 (dd, J = 8.4, 4.0 Hz, 1H, H_2), 2.74 (ddd, J = 8.5, 5.1, 3.7 Hz, 1H, H_3), 0.87 (dd, J = 3.8, 1.0 Hz, 1H, H_1). Spectroscopic data were consistent with those published previously.[90]

1a,7b-Dihydro-1H-cyclopropa[a]naphthalene-1-carbonyl chloride (3-4)

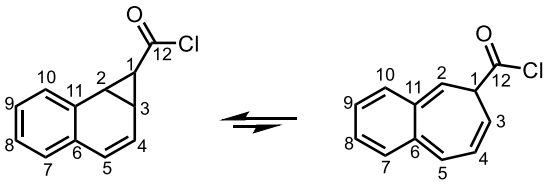

3-3 (100 mg, 0.54 mmol, 1 equiv.) was dissolved in anhydrous CH_2Cl_2 (2 mL). Oxalyl chloride (82 mg, 0.64 mmol, 1. equiv.) was added to the solution and the mixture was stirred at rt for 16 h. The solvent was removed *in vacuo* to yield the title compound as a yellow solid (101 mg, 0.50 mmol, 92%), which was used in subsequent reactions without further purification. **M.P.** ; **^{1}H NMR** (599 MHz, $CDCl_3$) δ 7.49 – 7.44 (m, 1H, H_{10}), 7.33 – 7.27 (m, 2H, H_8 and H_9), 7.22

– 7.14 (m, 1H, H_7), 6.51 (d, J = 9.5 Hz, 1H, H_5), 6.34 (dd, J = 9.5 , 5.1 Hz, 1H, H_4), 3.44 (dd, J = 8.7, 3.8 Hz, 1H, H_2), 3.02 (ddd, J = 8.5, 5.1, 3.4 Hz, 1H, H_3), 1.38 (t, J = 3.6 Hz, 1H, H_1); **^{13}C NMR** (151 MHz, $CDCl_3$) δ 176.0 (C_{12}), 131.2 (C_{11}), 130.8 (C_6), 129.2 (C_{10}), 128.5 (C_7), 128.4 (C_9), 127.9 (C_8), 127.6 (C_5), 124.7 (C_4), 35.4 (C_2), 33.5 (C_1), 32.6 (C_3); **HRMS-ASAP** m/z = 205.0417 $[M+H]^+$, calculated for $C_{12}H_{10}OCl$: 205.0420.

1,4,5,8,9,10-Hexahydroanthracene (3-9)

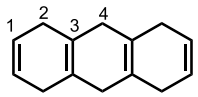

Anthracene (1.0 g, 5.61 mmol) was dissolved in dry THF (40 mL) and dry ethanol (12.5 mL, 0.22 mol). Liquid ammonia (40 mL) was added and the vigorously stirred suspension of anthracene was reduced with sodium (3.8 g, 0.165 mol) at –78 °C. The mixture was stirred for 20 h after which ammonia was allowed to evaporate as the temperature was raised to rt. Water (100 mL) was added to dissolve the inorganic salts completely. The product was extracted with Et_2O (3 × 50 mL) and the combined ether extracts were dried with anhydrous $MgSO_4$. The solvent was removed *in vacuo* and the crude residue was purified by recrystallization in benzene to yield the title compound as a colourless solid (835 mg, 4.53 mmol, 81%). **^{1}H NMR** (400 MHz, $CDCl_3$) δ 5.76 – 5.71 (m, 4H, H_1), 2.57 (d, J = 1.2 Hz, 8H, H_2), 2.43 (s, 4H, H_4). Spectroscopic data were consistent with those published previously.[126]

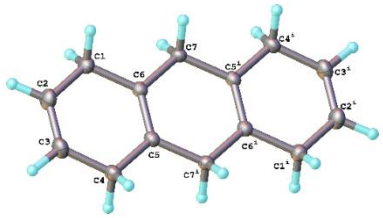

Crystal system: Monoclinic

Space group: P21/c

Unit cell parameters: a = 11.1353(3) Å; b = 4.40090(10) Å; c = 11.1311(4) Å; α = 90°; β = 114.7040(10); γ = 90°; V = 495.56(3) Å^3; Z = 2

Naphthalene-2,3-dicarbaldehyde (3-22a)

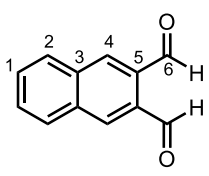

O-Phthaldialdehyde (1.0 g, 7.46 mmol, 1 equiv.) and 2,5-dimethoxy-tetrahydrofuran (1.0 g, 7.50 mmol, 1 equiv.) were dissolved in a mixture of 100% acetic acid (0.75 mL) and water (0.75 mL). One drop of piperidine was added and the reaction mixture was heated under reflux for 24 h. The mixture

was allowed to cool and the precipitate was filtered, washed with 10% HCl (10 mL), water (10 mL), methanol (10 mL) and ether (10 mL) to yield the title compound as an yellow solid (98 mg, 0.53 mmol, 7%). **^{1}H NMR** (400 MHz, $CDCl_3$) δ 10.65 (s, 2H, H_6), 8.47 (s, 2H, H_4), 8.11 – 8.01 (m, 2H, H_2), 7.78 – 7.72 (m, 2H, H_1). Spectroscopic data were consistent with those published previously.[132]

Anthracene-2,3-dicarbaldehyde (3-22b)

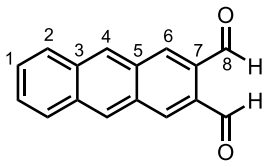

O-Phthaldialdehyde (6.0 g, 44.7 mmol, 1 equiv.) and 2,5-dimethoxytetrahydrofuran (12.0 g, 90.8 mmol, 2 equiv.) were dissolved in a mixture of 100% acetic acid (4.5 mL) and water (4.5 mL). 6 drops of piperidine were added and the reaction mixture was heated under at 120 °C for 24 h. The mixture was allowed to cool, the precipitate was washed with 10% HCl and water and filtered through a sintered glass funnel. The solid was then suspended in MeOH (25 mL), transferred to a 50 mL centrifuge tube and centrifuged at 10,000 rpm for 10 min. The supernatant was decanted, the solid remaining was resuspended in diethyl ether (25 mL) and centrifuged again at 10,000 rpm for 10 min. After decanting the supernatant, the solid residue was dried *in vacuo* to yield the title compound as a red solid (1.89 g, 8 mmol, 18%). **^{1}H NMR** (599 MHz, $CDCl_3$) δ 10.66 (s, 2H, H_8), 8.66 (s, 2H, H_4), 8.63 (s, 2H, H_6), 8.12 – 8.09 (m, 2H, H_2), 7.66 – 7.63 (m, 2H, H_1). Spectroscopic data were consistent with those published previously.[137]

Diethyl 8-oxo-8H-cyclohepta[b]naphthalene-7,9-dicarboxylate (3-24a)

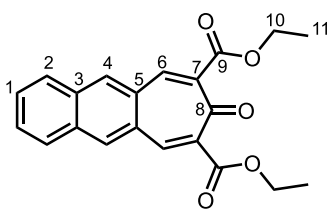

A mixture of **3-22a** (100 mg, 0.543 mmol, 1 equiv.), diethyl 1,3-acetonedicarboxylate (109 mg, 0.539 mmol, 1 equiv.) and piperidine acetate (4 mg, 0.027 mmol, 5 mol%) was dissolved in toluene (3 mL). The mixture was heated to reflux before one drop of piperidine was added. The mixture was heated further for 2 h and allowed to cool. After evaporation, the crude residue was purified by column chromatography (Teledyne Isco CombiFlash Rf+ system, 24 g SiO_2, hexane−EtOAc, gradient elution) to yield the title compound as an orange solid (105 mg, 0.299 mmol, 55%). **^{1}H NMR**

(400 MHz, $CDCl_3$) δ 8.29 (s, 2H, H_4), 8.26 (s, 2H, H_6), 8.01 (dd, *J* = 6.2, 3.3 Hz, 2H, H_2), 7.70 (dd, *J* = 6.2, 3.1 Hz, 2H, H_1), 4.42 (q, *J* = 7.0 Hz, 4H, H_{10}), 1.42 (t, *J* = 7.1 Hz, 6H, H_{11}). ^{13}C NMR data and melting point are yet to be determined.

Diethyl 9-oxo-9H-cyclohepta[b]anthracene-8,10-dicarboxylate (3-24b)

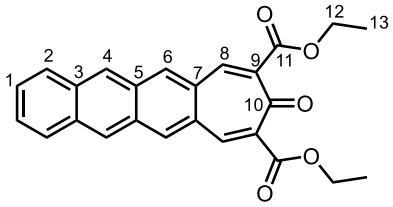

A solution of diethyl-1,3-acetonedicarboxylate (1 mL, 5.5 mmol, 1 equiv.) in toluene (15 mL) was added dropwise over 30 min to a solution of anthracene-2,3-dicarbaldehyde (1.3 g, 5.5 mmol, 1 equiv), piperidine (0.1 mL, 1.4 mmol, 25 mol%) , and acetic acid (0.3 mL, 4.8 mmol, 0.87 equiv.) in toluene (100 mL). The reaction was heated at reflux for 16 h and allowed to cool. After evaporation, the crude residue was purified by column chromatography (Teledyne Isco CombiFlash Rf+ system, 220 g SiO2, CH_2Cl_2−MeOH, gradient elution). The brown residue obtained was washed with diethyl ether to remove residual MeOH, and the solid remaining was suspended in toluene (25 mL) and centrifuged at 10,000 rpm for 10 min. After decanting the supernatant, the solid residue was dried *in vacuo* to yield the title compound as an orange solid (661 mg, 1.65 mmol, 30%). **M.P.** 196-198 °C; **^{1}H NMR** (599 MHz, $CDCl_3$) δ 8.57 (s, 2H, H_4), 8.43 (s, 2H, H_6), 8.22 (s, 2H, H_8), 8.09 – 8.05 (m, 2H, H_2), 7.60 – 7.57 (m, 2H, H_1), 4.40 (q, *J* = 7.2 Hz, 4H, H_{12}), 1.41 (t, *J* = 7.2 Hz, 6H, H_{13}); **^{13}C NMR** (151 MHz, $CDCl_3$) δ 184.9 (C_{10}), 166.4 (C_{11}), 142.7 (C_8), 137.3 (C_6), 134.5 (C_9), 133.4 (C_3), 130.8 (C_5), 129.9 (C_7), 128.7 (C_2), 128.0 (C_4), 127.4 (C_1), 62.0 (C_{12}), 14.3 (C_{13}); **HRMS-ASAP** *m/z* = 401.1396 [M+H]+, calculated for $C_{25}H_{21}O_5$: 401.1389; **UV-VIS** (CH_2Cl_2, 80 μM, 298 K).

9H-Cyclohepta[b]anthracen-9-one (3-25b)

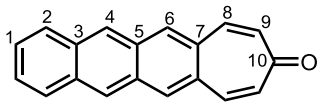

3-24b (31 mg, 0.078 mmol) was dissolved in 5% KOH in methanol solution (1 mL) and the mixture was heated under reflux for 4 h. After cooling the mixture was extracted with CH_2Cl_2 (3 × 15 mL) and the combined organic extracts were dried over anhydrous $MgSO_4$ and evaporated. The crude residue was purified by column chromatography (Teledyne Isco CombiFlash Rf+ system, 12 g SiO_2, hexane−EtOAc, gradient elution) to yield the title compound as an impure yellow

solid (17 mg). **^{1}H NMR** (400 MHz, $CDCl_3$) δ 8.60 (s, 2H, H_4), 8.37 (s, 2H, H_6), 8.12 – 8.07 (m, 2H, H_2), 7.62 – 7.59 (m, 2H, H_1), 7.59 – 7.56 (m, 2H, H_8 or H_9), 6.68 – 6.62 (m, 2H, H_8 or H_9); **HRMS-ASAP** *m/z* = 257.0954 $[M+H]^+$, calculated for $C_{19}H_{13}O$: 257.0966. ^{13}C NMR data and melting point are yet to be determined.

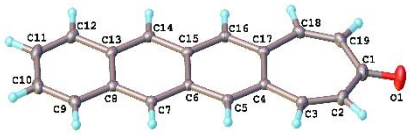

Crystal system: Monoclinic

Space group: P21/c

Unit cell parameters: a = 6.2394(2) Å; b = 7.4786(2) Å; c = 26.0422(8) Å; α = 90°; β = 90.317(1); γ = 90°; V = 1215.16(6) Å^3; Z = 4

Tetraethyl 9, 15-dihydroxy-8, 11-dihydro-7H-7, 11-prop[1]enocyclohepta[b]anthracene-8, 10,14,16-tetracarboxylate (3-29)

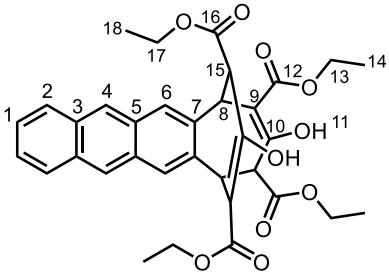

A solution of diethyl-1,3-acetonedicarboxylate (1.6 mL, 8.5 mmol, 2 equiv.) in toluene (15 mL) was added dropwise over 30 min to a solution of anthracene-2,3-dicarbaldehyde (1 g, 4.3 mmol, 1 equiv), piperidine (0.1 mL, 1.4 mmol, 0.3 equiv.), and acetic acid (0.3 mL, 4.8 mmol, 1.1 equiv.) in toluene (100 mL). The reaction was heated at reflux for 16 h and allowed to cool. After evaporation, the crude residue was purified by column chromatography (Teledyne Isco CombiFlash Rf+ system, 220 g SiO2, CH_2Cl_2–MeOH, gradient elution to yield the title compound as an yellow solid (721 mg, 1.2 mmol, 28%). **^{1}H NMR** (400 MHz, $CDCl_3$, 298 K) δ 13.34 (s, 2H, H_{11}), 8.32 (s, 2H, H_4), 7.99 (dd, *J* = 6.5, 3.3 Hz, 2H, H_2), 7.74 (s, 2H, H_6), 7.48 (dd, *J* = 6.5, 3.3 Hz, 2H, H_1), 4.87 (d, *J* = 4.6 Hz, 2H, H_{15}), 4.49 – 4.40 (m, 4H, H_{13} or H_{17}), 3.95 – 3.89 (m, 2H, H_8), 3.87 – 3.66 (m, 4H, H_{13} or H_{17}), 1.51 (q, *J* = 7.1 Hz, 6H, H_{14} or H_{18}), 0.73 (t, *J* = 7.1 Hz, 6H, H_{14} or H_{18}).

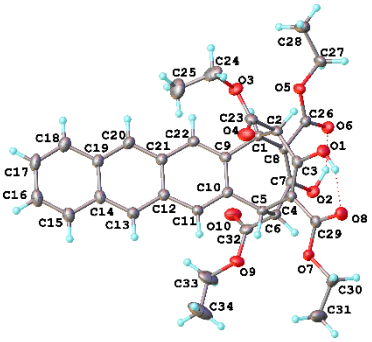

Crystal system: Triclinic

Space group: P-1

Unit cell parameters: a = 10.0644(3) Å; b = 10.2498(3) Å; c = 17.0767(5) Å; α = 76.2030(10)°; β = 82.3180(10)°; γ = 61.7600(10)°; V = 1506.70(8) Å^3; Z = 2

5H-cyclohepta[b]anthracene-5,9,13-trione (3-30)

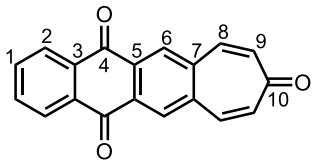

A solution of **3-25b** (~ 5 mg) in deuterated chloroform was left under ambient temperature and lighting for 10 days to yield an oxidised derivative. **^{1}H NMR** (400 MHz, $CDCl_3$, 298 K) δ 8.21 (s, 2H, H_6), 8.00 (dd, J = 6.3, 3.2 Hz, 2H, H_2), 7.67 (dd, J = 6.3, 3.2 Hz, 2H, H_1), 7.62 – 7.59 (m, 2H, H_9), 6.77 – 6.70 (m, 2H, H_8).

Diethyl 5,9,13-trioxo-9,13-dihydro-5H-cyclohepta[b]anthracene-8,10-dicarboxylate

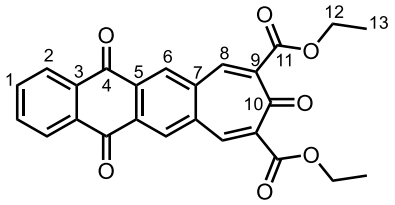

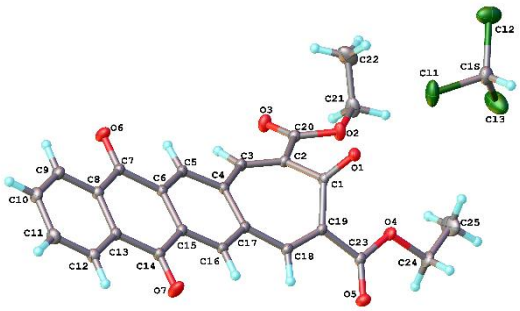

Crystal system: Monoclinic

Space group: P21/c

Unit cell parameters: a = 16.7677(4) Å; b = 14.8509(4) Å; c = 9.7007(3) Å; α = 90°; β = 92.5626(10)°; γ = 90°; V = 2413.21(11) Å^3; Z = 4

6. References

1 International Energy Agency, 'Solar PV – Analysis', https://www.iea.org/reports/solar-pv.
2 A. E. Becquerel, *Comptes Rendus l'Academie des Sci.*, 1839, **9**, 561–567.
3 D. Lincot, *Comptes Rendus Phys.*, 2017, **18**, 381–390.
4 C. E. Fritts, *Am. J. Sci.*, 1883, **s3-26**, 465–472.
5 D. M. Chapin, C. S. Fuller and G. L. Pearson, *Bell Lab.*, 1957, 2780765.
6 M. A. Green, *Prog. Photovoltaics Res. Appl.*, 2005, **13**, 447–455.
7 B. Goldstein, *Phys. Rev.*, 1958, **109**, 601–603.
8 K. W. J. Barnham and G. Duggan, *J. Appl. Phys.*, 1990, **67**, 3490–3493.
9 A. Kojima, K. Teshima, Y. Shirai and T. Miyasaka, *J. Am. Chem. Soc.*, 2009, **131**, 6050–6051.
10 N. Kaur, M. Singh, D. Pathak, T. Wagner and J. M. Nunzi, *Synth. Met.*, 2014, **190**, 20–26.
11 W. Shockley and H. J. Queisser, *J. Appl. Phys.*, 1961, **32**, 510–519.
12 A. J. Carrod, V. Gray and K. Börjesson, *Energy Environ. Sci.*, 2022, **15**, 4982–5016.
13 L. C. Hirst and N. J. Ekins-Daukes, *Prog. Photovoltaics Res. Appl.*, 2011, **19**, 286–293.
14 H. Heidarzadeh, A. Rostami and M. Dolatyari, *Mater. Sci. Semicond. Process.*, 2020, **109**, 104936.
15 A. Wang and Y. Xuan, *Energy*, 2018, **144**, 490–500.
16 J. Zhao, A. Wang and M. A. Green, *Sol. Energy Mater. Sol. Cells*, 2001, **65**, 429–435.
17 A. De Vos, *J. Phys. D. Appl. Phys.*, 1980, **13**, 839.
18 J. F. Geisz, R. M. France, K. L. Schulte, M. A. Steiner, A. G. Norman, H. L. Guthrey, M. R. Young, T. Song and T. Moriarty, *Nat. Energy 2020 54*, 2020, **5**, 326–335.
19 S. Sundaram, D. Benson and T. K. Mallick, *Sol. Photovolt. Technol. Prod.*, 2016, 7–22.
20 M. C. Hanna and A. J. Nozik, *J. Appl. Phys.*, 2006, **100**, 074510.
21 M. B. Smith and J. Michl, *Annu. Rev. Phys. Chem.*, 2013, **64**, 361–386.
22 S. Singh, W. J. Jones, W. Siebrand, B. P. Stoicheff and W. G. Schneider, *J. Chem. Phys.*, 1965, **42**, 330–342.
23 C. E. Swenberg and W. T. Stacy, *Chem. Phys. Lett.*, 1968, **2**, 327–328.
24 S. Ito, T. Nagami and M. Nakano, *J. Photochem. Photobiol. C Photochem. Rev.*, 2018, **34**, 85–120.
25 H. Rademaker, A. J. Hoff, R. Van Grondelle and L. N. M. Duysens, *Biochim. Biophys. Acta - Bioenerg.*, 1980, **592**, 240–257.
26 R. H. Austin, G. L. Baker, S. Etemad and R. Thompson, *J. Chem. Phys.*, 1989, **90**, 6642–6646.
27 M. B. Smith and J. Michl, *Chem. Rev.*, 2010, **110**, 6891–6936.
28 R. Casillas, I. Papadopoulos, T. Ullrich, D. Thiel, A. Kunzmann and D. M. Guldi, *Energy Environ. Sci.*, 2020, **13**, 2741–2804.
29 A. J. Baldacchino, M. I. Collins, M. P. Nielsen, T. W. Schmidt, D. R. McCamey and M. J. Y. Tayebjee, , DOI:10.48550/arxiv.2202.01326.
30 Y. Jiang, M. P. Nielsen, A. J. Baldacchino, M. A. Green, D. R. McCamey, M. J. Y. Tayebjee, T. W. Schmidt and N. J. Ekins-Daukes, *Prog. Photovoltaics Res. Appl.*, 2021, **29**, 899–906.
31 S. M. Menke, N. A. Ran, G. C. Bazan and R. H. Friend, *Joule*, 2018, **2**, 25–35.
32 R. W. Macqueen, M. Liebhaber, J. Niederhausen, M. Mews, C. Gersmann, S. Jäckle, K. Jäger, M. J. Y. Tayebjee, T. W. Schmidt, B. Rech and K. Lips, *Mater. Horizons*, 2018, **5**, 1065–1075.
33 M. Einzinger, T. Wu, J. F. Kompalla, H. L. Smith, C. F. Perkinson, L. Nienhaus, S. Wieghold, D. N. Congreve, A. Kahn, M. G. Bawendi and M. A. Baldo, *Nature*, 2019, **571**, 90–94.
34 G. P. Moss, P. A. S. Smith and D. Tavernier, *Pure Appl. Chem.*, 1995, **67**, 1307–1375.
35 R. Dorel and A. M. Echavarren, *Eur. J. Org. Chem.*, 2017, **2017**, 14–24.
36 S. Yoo, B. Domercq and B. Kippelen, *Appl. Phys. Lett.*, 2004, **85**, 5427–5429.
37 S. A. Odom, S. R. Parkin and J. E. Anthony, *Org. Lett.*, 2003, **5**, 4245–4248.
38 C. Wang, H. Dong, W. Hu, Y. Liu and D. Zhu, *Chem. Rev.*, 2012, **112**, 2208–2267.
39 E. Hückel, *Zeitschrift für Phys.*, 1931, **70**, 204–286.
40 R. Mondal, C. Tönshoff, D. Khon, D. C. Neckers and H. F. Bettinger, *J. Am. Chem. Soc.*, 2009, **131**, 14281–14289.
41 A. Jančařík, J. Holec, Y. Nagata, M. Šámal and A. Gourdon, *Nat. Commun. 2022 131*, 2022, **13**, 1–7.
42 F. Eisenhut, T. Kühne, F. García, S. Fernández, E. Guitián, D. Pérez, G. Trinquier, G. Cuniberti, C. Joachim, D. Peña and F. Moresco, *ACS Nano*, 2020, **14**, 1011–1017.
43 E. Clar, *The aromatic sextet.*, Wiley-Interscience, London, 1972.
44 M. Solà, *Front. Chem.*, 2013, **1**, 22.
45 H. F. Bettinger, *Pure Appl. Chem.*, 2010, **82**, 905–915.
46 K. J. Thorley and J. E. Anthony, *Isr. J. Chem.*, 2014, **54**, 642–649.
47 T.-G. Hsu, H.-C. Chou, M.-J. Liang, Y.-Y. Lai and Y.-J. Cheng, *Chem. Commun.*, 2019, **55**, 381–384.
48 L. B. Roberson, J. Kowalik, L. M. Tolbert, C. Kloc, R. Zeis, X. Chi, R. Fleming and C. Wilkins, *J. Am.*

Chem. Soc., 2005, **127**, 3069–3075.
49 M. Watanabe, Y. J. Chang, S.-W. Liu, T.-H. Chao, K. Goto, M. Islam, C.-H. Yuan, Y.-T. Tao, T. Shinmyozu and T. J. Chow, *Nat. Chem.*, 2012, **4**, 574–578.
50 C. S. Foote, *Acc. Chem. Res.*, 1968, **1**, 104–110.
51 S.-H. Chien, M.-F. Cheng, K.-C. Lau and W.-K. Li, *J. Phys. Chem.*, 2005, **109**, 7509–7518.
52 A. R. Reddy and M. Bendikov, *Chem. Commun.*, 2006, 1179.
53 W. Fudickar and T. Linker, *J. Am. Chem. Soc.*, 2012, **134**, 15071–15082.
54 I. Kaur, W. Jia, R. P. Kopreski, S. Selvarasah, M. R. Dokmeci, C. Pramanik, N. E. McGruer and G. P. Miller, *J. Am. Chem. Soc.*, 2008, **130**, 16274–16286.
55 K. Ono, H. Totani, T. Hiei, A. Yoshino, K. Saito, K. Eguchi, M. Tomura, J. ichi Nishida and Y. Yamashita, *Tetrahedron*, 2007, **63**, 9699–9704.
56 Y. Li, Y. Wu, P. Liu, Z. Prostran, S. Gardner and B. S. Ong, *Chem. Mater.*, 2007, **19**, 418–423.
57 S. Z. Bisri, T. Takenobu, T. Takahashi and Y. Iwasa, *Appl. Phys. Lett.*, 2010, **96**, 183304.
58 D. A. da Silva Filho, E.-G. Kim and J.-L. Brédas, *Adv. Mater.*, 2005, **17**, 1072–1076.
59 J. E. Anthony, *Angew. Chem. Int. Ed.*, 2008, **47**, 452–483.
60 M. Dvořák, S. K. K. Prasad, C. B. Dover, C. R. Forest, A. Kaleem, R. W. Macqueen, A. J. Petty, R. Forecast, J. E. Beves, J. E. Anthony, M. J. Y. Tayebjee, A. Widmer-Cooper, P. Thordarson and T. W. Schmidt, *J. Am. Chem. Soc.*, 2021, **143**, 13749–13758.
61 A. Maliakal, K. Raghavachari, H. Katz, E. Chandross and T. Siegrist, *Chem. Mater.*, 2004, **16**, 4980–4986.
62 J. E. Anthony, J. S. Brooks, D. L. Eaton and S. R. Parkin, *J. Am. Chem. Soc.*, 2001, **123**, 9482–9483.
63 Z. Stewart, *Lewis Honor. Coll. Capstone Collect.*, 2013, 11.
64 J. M. Luther and J. C. Johnson, *Nature*, 2019, **571**, 38–39.
65 T. Rahman, R. S. Bonilla, A. Nawabjan, P. R. Wilshaw and S. A. Boden, *Sol. Energy Mater. Sol. Cells*, 2017, **160**, 444–453.
66 K. Hafner, *Angew. Chem. Int. Ed. Engl.*, 1964, **3**, 165–173.
67 D. J. M. Lyons, R. D. Crocker, M. Blümel and T. V Nguyen, *Angew. Chem. Int. Ed.*, 2017, **56**, 1466–1484.
68 G. Merling, *Berichte der Dtsch. Chem. Gesellschaft*, 1891, **24**, 3108–3126.
69 B. D. Kelly and T. H. Lambert, *J. Am. Chem. Soc.*, 2009, **131**, 13930–13931.
70 B. Ye and N. Cramer, *Science (80-.).*, 2012, **338**, 504–506.
71 W. von E. Doering and L. H. Knox, *J. Am. Chem. Soc.*, 1954, **76**, 3203–3206.
72 F. Hoffmann, G. W. Fester and J. Wagler, *Zeitschrift fur Naturforsch. - Sect. B J. Chem. Sci.*, 2010, **65**, 1137–1142.
73 W. G. Fateley and E. R. Lippincott, *J. Am. Chem. Soc.*, 1955, **77**, 249–250.
74 H. J. Dauben, F. A. Gadecki, K. M. Harmon and D. L. Pearson, *J. Am. Chem. Soc.*, 1957, **79**, 4557–4558.
75 C. A. Bunton, F. Davoudazedeh and W. E. Watts, *J. Am. Chem. Soc.*, 1981, **103**, 3855–3858.
76 T. Shono, T. Nozoe, H. Maekawa and S. Kashimura, *Tetrahedron Lett.*, 1988, **29**, 555–558.
77 D. H. Geske, *J. Am. Chem. Soc.*, 1959, **81**, 4145–4147.
78 F. A. L. Anet, *J. Am. Chem. Soc.*, 1964, **86**, 458–460.
79 S. S. Butcher, *J. Chem. Phys.*, 1965, **42**, 1833–1836.
80 W. H. Donovan and W. E. White, *J. Org. Chem.*, 1996, **61**, 969–977.
81 A. Ladenburg, *Berichte der Dtsch. Chem. Gesellschaft*, 1881, **14**, 2126–2131.
82 R. Willstätter, *Justus Liebigs Ann. Chem.*, 1901, **317**, 204–265.
83 M. L. H. Green and D. K. P. Ng, *Chem. Rev.*, 1995, **95**, 439–473.
84 W. Abraham, L. Grubert, S. Schmidt-Schäffer and K. Buck, *Eur. J. Org. Chem.*, 2005, **2005**, 374–386.
85 N. Liu, W. Song, C. M. Schienebeck, M. Zhang and W. Tang, *Tetrahedron*, 2014, **70**, 9281–9305.
86 E. Buchner and T. Curtius, *Berichte der Dtsch. Chem. Gesellschaft*, 1885, **18**, 2377–2379.
87 T. Curtius, *Berichte der Dtsch. Chem. Gesellschaft*, 1883, **16**, 2230–2231.
88 J. F. Liebman and A. Greenberg, *Chem. Rev.*, 1989, **89**, 1225–1246.
89 A. J. Anciaux, A. Demonceau, A. F. Noels, A. J. Hubert, R. Warin and P. Teyssié, *J. Org. Chem.*, 1981, **46**, 873–876.
90 P. Müller, J. L. Toujas and G. Bernardinelli, *Helv. Chim. Acta*, 2000, **83**, 1525–1534.
91 M. J. S. Dewar and C. R. Ganellin, *J. Chem. Soc.*, 1959, **41**, 3139–3144.
92 E. Vogel, W. Wiedemann, H. Kiefer and W. F. Harrison, *Tetrahedron Lett.*, 1963, **4**, 673–678.
93 F. R. Jensen and L. A. Smith, *J. Am. Chem. Soc.*, 1964, **86**, 956–957.
94 J. M. Assour and S. E. Harrison, *J. Am. Chem. Soc.*, 1965, 87, 652–653.
95 R. Wehner and H. Günther, *J. Am. Chem. Soc.*, 1975, 97, 923–924.
96 R. Hoffmann, *Tetrahedron Lett.*, 1970, **11**, 2907–2909.
97 T. Clark, G. W. Spitznagel, R. Klose and P. v. R. Schleyer, *J. Am. Chem. Soc.*, 1984, **106**, 4412–4419.

98 H. E. Winberg, *J. Org. Chem.*, 1959, **24**, 264–265.
99 D. K. Mandal, in *Pericyclic Chemistry*, Elsevier, 2018, pp. 63–106.
100 R. B. Woodward and R. Hoffmann, *Angew. Chem. Int. Ed. Engl.*, 1969, **8**, 781–853.
101 D. N. Reinhoudt, M. P. Smael, W. J. M. van Tilborg and J. P. Visser, *Tetrahedron Lett.*, 1973, **14**, 3755–3758.
102 K. Kamikawa, Y. Shimizu, H. Matsuzaka and M. Uemura, *J. Organomet. Chem.*, 2005, **690**, 5922–5928.
103 N. Tsukada, Y. Sakaihara and Y. Inoue, *Tetrahedron Lett.*, 2007, **48**, 4019–4021.
104 C. M. Older, R. McDonald and J. M. Stryker, *J. Am. Chem. Soc.*, 2005, **127**, 14202–14203.
105 W.-M. Shu, J.-R. Ma, Y. Yang and A.-X. Wu, *Org. Lett*, 2014, **16**, 44.
106 E. Heilbronner and A. Eschenmoser, *Helv. Chim. Acta*, 1953, **36**, 1101–1109.
107 M. Allan, E. Heilbronner and E. Kloster-Jensen, *J. Electron Spectros. Relat. Phenomena*, 1975, **6**, 181–205.
108 G. Naville, H. Strauss and E. Heilbronner, *Helv. Chim. Acta*, 1960, **43**, 1221–1243.
109 K. C. Srivastava and S. Dev, *Tetrahedron*, 1972, **28**, 1083–1091.
110 G. Berti, *J. Org. Chem.*, 1957, **22**, 230.
111 K. Komatsu, R. Tsuji and K. Takeuchi, *Tetrahedron Lett.*, 1989, **30**, 4689–4692.
112 R. L. Danheiser, B. R. Dixon and R. W. Gleason, *J. Org. Chem.*, 1992, **57**, 6094–6097.
113 I. D. Reingold, H. A. Trujillo and B. E. Kahr, *J. Org. Chem.*, 1986, **51**, 1627–1629.
114 P. R. McGonigal, C. de León, Y. Wang, A. Homs, C. R. Solorio-Alvarado and A. M. Echavarren, *Angew. Chem. Int. Ed.*, 2012, **51**, 13093–13096.
115 S. I. Naya, H. Ohtoshi and M. Nitta, *J. Org. Chem.*, 2006, **71**, 176–184.
116 A. B. Skov, S. L. Broman, A. S. Gertsen, J. Elm, M. Jevric, M. Cacciarini, A. Kadziola, K. V. Mikkelsen and M. B. Nielsen, *Chem. - A Eur. J.*, 2016, **22**, 14567–14575.
117 S. T. Olsen, T. Hansen and K. V. Mikkelsen, *J. Phys. Chem. C*, 2015, **119**, 14829–14833.
118 J. Wang, M. Xiao, W. Chen, M. Qiu, Z. Du, W. Zhu, S. Wen, N. Wang and R. Yang, *Macromolecules*, 2014, **47**, 7823–7830.
119 R. Kumar, H. Aggarwal and A. Srivastava, *Chem. – A Eur. J.*, 2020, **26**, 10653–10675.
120 H. H. Rennhard, G. Di Modica, W. Simon, E. Heilbronner and A. Eschenmoser, *Helv. Chim. Acta*, 1957, **40**, 957–968.
121 M. J. S. Dewar and C. R. Ganellin, *J. Chem. Soc.*, 1959, 2438.
122 F. Seel, *Zeitschrift für Anorg. und Allg. Chemie*, 1943, **250**, 331–351.
123 A. N. Nesmejaow and E. J. Kahn, *Berichte der Dtsch. Chem. Gesellschaft*, 1934, **67**, 372.
124 R. G. Johnson and R. K. Ingham, *Chem. Rev.*, 1956, **56**, 219–269.
125 J. K. Kochi, *J. Am. Chem. Soc.*, 1965, **87**, 2500–2502.
126 G. Mehta, S. Sen and S. S. Ramesh, *Eur. J. Org. Chem.*, 2007, **2007**, 423–436.
127 W. J. Gensler, J. P. Marshall, J. J. Langone and J. C. Chen, *J. Org. Chem.*, 1977, **42**, 118–125.
128 S. Mashraqui and P. Keehn, *Synth. Commun.*, 1982, **12**, 637–645.
129 E. C. Friedrich and F. Niyati-Shirkhodaee, *J. Org. Chem.*, 1991, **56**, 2202–2205.
130 E. C. Friedrich and E. J. Lewis, *J. Org. Chem.*, 1990, **55**, 2491–2494.
131 K. Kitamura, R. Kudo, H. Sugiyama, H. Uekusa and T. Hamura, *Chem. Commun.*, 2020, **56**, 14988–14991.
132 C. F. Wilcox and K. A. weber, *J. Org. Chem.*, 1986, **51**, 1088–1094.
133 A. Mallouli and Y. Lepage, *Synth.*, 1980, **1980**, 689.
134 John Wiley & Sons, Ltd, *Arch. Pharm. (Weinheim).*, 1988, 321, 765–766.
135 J. L. Luche, *J. Am. Chem. Soc.*, 1978, **100**, 2226–2227.
136 O. Berg, E. L. Chronister, T. Yamashita, G. W. Scott, R. M. Sweet and J. Calabrese, , DOI:10.1021/jp984066g.
137 C.-H. Lin, K.-H. Lin, B. Pal and L.-D. Tsou, *Chem. Commun.*, 2009, 803–805.
138 L. M. Bateman, O. A. McNamara, N. R. Buckley, P. O'Leary, F. Harrington, N. Kelly, S. O'Keeffe, A. Stack, S. O'Neill, D. G. McCarthy and A. R. Maguire, *Org. Biomol. Chem.*, 2015, **13**, 11026–11038.

7. CDT Trainings and Seminars

Talks and research seminars attended

Date	Topic	Speaker
13/10/2020	The whole energy system's view of energy, and the role of buildings within it	Dr Sara Walker, Newcastle University
21/10/2020	Substituted shape-shifters and 8π/6π synthesis	Dr Thomas Fallon, University of Adelaide
10/11/2020	The BP-ICAM: Materials challenges in low carbon	Sheetal Handa, BP
10/11/2020	The Stirling Protocol – Putting the environment at the heart of prosperity & social inclusion	Maggie Cusack, University of Sterling
13/11/2020	Unclear nuclear future	Brian Matthews, Durham Energy Institute
25/11/2020	Much ado about a ring: The curious case of tropylium ion	Dr Vinh Nguyen, University of New South Wales
17/03/2021	Linking Structure and Function in Materials for Energy and the Environment	Dr John Griffin, Lancaster University
15/10/2021	Smart energy systems: AI applications and living labs	Professor Zhong Fan, Keele University
16/02/2022	An introduction to off grid net zero electricity generation for gas applications	Revolution Turbine Technologies Ltd.

Attended lectures provided by RENU CDT (2 hours each)

Date	Topic	Speaker
19/10/2020	Semiconductor electrochemistry: introduction & characterization techniques	Dr Devendra Tiwari, Northumbria University
19/10/2020	Photochemistry and photocatalysis	Dr Elizabeth Gibson, Newcastle Unversity
20/10/2020	Electrochemistry: (Fundamental of electrochemistry) and its applications in sustainable energy systems	Dr Shahid Rasul, Northumbria University
21/10/2020	Solar PV: Fundamentals, materials, devices and systems	Professor Neil Beattie, Northumbria University
22/10/2020	Fabrications of Solar PVs	Dr Guillaume Zoppi, Northumbria University
23/10/2020	Nanomaterials and nanotechnology	Professor Lidija Siller, Newcastle University
23/10/2020	Polyoxometalates Chemistry: Applications in Energy Materials	Dr John Errington, Newcastle University
27/10/2020	Electron micro-spectroscope SEM/TEM	Dr Budhika Mendis, Durham University

28/10/2020	Batteries and electric vehicles	Dr Terence Liu, Northumbria University
02/11/2020	Structure and Spectroscopies (XPS, Raman, XRD, Scanned Probe Microscopy)	Dr Michael Hunt, Durham University
02/11/2020	Solid-State NMR Spectroscopy	Dr Karen Johnston, Durham University
04/11/2020	Aerodynamics of Wind Energy	Dr Majid Bastankhah, Durham University
05/11/2020	Understanding Societal responsibility for Climate Change: Involving public in solution	Professor Lynn Frewer, Newcastle University
23/11/2020	RSC – Publishing and How to Publish	Dr Bianca Provost, Roayl Society of Chemistry
02/12/2020	Solar thermal energy storage	Dr Carolina Costa, Northumbria University
18/01/2021	PV systems and applications	Professor Nicola Pearsall, Northumbria University
20/01/2021	Impact of climate change	Professor Chris Stokes, Durham University
20/01/2021	Decarbonisation of heating & cooling	Dr Andrew Smallbone, Durham University
21/01/2021	Low carbon Energy for development	Dr Ben Campbell, Durham University
21/01/2021	The global rise of zero liquid discharge for wastewater management: A case study from the brewing industry	Dr Marloes Peeters, Newcastle University
20/05/2021	Optical properties of materials	Dr Elizabeth Gibson, Newcastle Unversity
28/05/2021	Current-voltage and External Quantum Efficiency Measurement of Solar Cells	Dr Yongtao Qu, Northumbria University

ReNU CDT Workshops attended

Date	**Workshop**
08/10/2020 – 04/12/2020	Errors and uncertainties lecture course and workshops
29-30/10/2020	Responsible Research & Innovation Hackathon
11/11/2020	Outreach training
12/11/2020	Equality, diversity & inclusion training
12/11/2020	Innovation training
27/11/2020	Impact training
30/11/2020 – 01/12/2020	Python Training
08/03/2021–19/03/2021	2-week Innovation Challenge: Creating a business model
25/03/2021 and 01/04/2021	‘Welcome to Westminister’ – Policy making training
15/10/2021 − 23/11/2021	Extended mini group research project on whole energy systems
09/04/2022 – 09/05/2022	Extended mini group research project – Industry challenge